Filamentary Magnetohydrodynamic Plasmas

R. Kinney[1,3], T. Tajima[1], J. C. McWilliams[2], N. Petviashvili[1]

Abstract

We develop a filamentary construct of magnetohydrodynamical plasma dynamics based on the Elsasser variables. This approach is modeled after discrete vortex models of hydrodynamical turbulence, which cannot be expected in general to produce results identical to ones based on a Fourier decomposition of the fields. In a highly intermittent plasma, the induction force is small compared to the convective motion, and when this force is neglected, the plasma vortex system is described by a Hamiltonian. For a system with many such vortices, we present a statistical treatment of a collection of discrete current-vorticity concentrations. Canonical and microcanonical statistical calculations show that both the vorticity and the current spectra are peaked at long wavelengths, and the expected states revert to known hydrodynamical states as the magnetic field vanishes. These results differ from previous Fourier-based statistical theories, but it is found that when the filament calculation is expanded to include the inductive force, the results approach the Fourier equilibria in the low-temperature limit, and the previous Hamiltonian plasma vortex results in the high-temperature limit. Numerical simulations of a large number of filaments are carried out and support the theory. A three-dimensional vortex model is outlined as well, which is also Hamiltonian when the inductive force is neglected. A statistical calculation in the canonical ensemble

[1]Institute for Fusion Studies, University of Texas at Austin, Austin, TX 78712
[2]National Center for Atmospheric Research, Boulder, CO 80307
[3]Present address: Advanced Study Program, NCAR, Boulder, CO 80307

and numerical simulations show that a non-zero large-scale magnetic field is statistically favored, and that the preferred shape of this field is a long, thin tube of flux. Possible applications to a variety of physical phenomena are suggested.

I. Introduction

Because of the engineering problem of maintaining a confined ionized gas, the traditional theoretical approach to describing plasmas has been to identify stable and unstable configurations. While such knowledge may tell the experimentalist what to avoid building, it does not help the theorist understand what the naturally-occurring states of a plasma are. For such knowledge, a probabilistic approach is necessary.[1-3] Since at a fundamental level any fluid is no more than a collection of particles, one might naively expect a fluid's equilibrium states to conform to the Gaussian of "true" thermodynamic equilibrium. Presumably after sufficient time, and in the absence of external influences, any fluid should eventually reach such an equilibrium, but how long must one wait, and what transpires meanwhile? The time required for the particles to reach their ultimate distribution may be extremely long, and they may occupy some quite long-lived states in the interim. Indeed, if a fluid description is appropriate for a given system, then any statistical analysis of that system should be based on the fluid equations, which will produce states quite different from a particle model.

Statistical tools for continuous systems, unfortunately, barely exist at the moment.[4] To perform statistical mechanics on a fluid system, some discrete representation must be chosen. That the results of the discrete system will approach the continuous system in some limit must be taken on faith. A point of great subtlety is that discrete representations of continuous objects are in no sense unique, and results obtained via one representation may be quite different from those obtained through another.[5]

Two discrete representations which have been shown to be effective in modeling ideal hydrodynamical turbulence in two dimensions are a Fourier-mode representation and a discrete-vortex representation.[6] The two approaches do not yield identical results, but both display interesting thermodynamical features in that the temperature is allowed to be negative (in two dimensions), and the system exhibits self-organizational tendencies. While both ap-

proaches enjoy a firm mathematical basis, the question remains of which gives a more realistic description of a physical fluid. This question may be only resolvable phenomenologically.

There is a well-known tendency for a fluid to form intermittent structures when dissipation is small. In addition to casual observations of naturally-occurring vortices in day-to-day life, experimental observations of thin films of superfluid Helium[48] have been rich in vortex structure. Very high-resolution, spectral-based numerical simulations of high Reynolds-number[7,8] fluids have consistently shown a tendency towards intermittency, specifically a formation of sharply peaked axisymmetric vortex filaments which are quite persistent in time. While such structures can be represented by Fourier modes, the phase correlations represented by their coherence are very difficult to treat in a statistical theory. Present statistical theories based on a truncated Fourier representation are unable to predict the formation of these filaments, the presence of which has significant effects on dynamical quantities such as cascade rates.[9]

The case for intermittent structures in plasmas is equally strong, if not stronger. An analysis of two-dimensional magnetohydrodynamics (MHD) using a closure method[10] shows that a cascade of current to small wavelengths is to be expected, with singularities formed in finite time from smooth initial conditions. Since strongly intermittent magnetic fields were first observed in the solar atmosphere,[11] much evidence of intermittent, filamentary plasma structures has been found in many astrophysical plasmas.[12-15] Laboratory plasmas have also displayed key features indicating intermittency,[16] and two-dimensional spectral fluid simulations at high resolution[17-19] have shown strongly peaked structures in both current and vorticity.

The purpose of this work is to describe a representation of ideal MHD that employs singular structures as its fundamental objects. We introduce a two-dimensional, discrete-vortex formalism for MHD in section 2, and predict its probable states, for filaments with fixed strengths in section 3, and for filaments whose strength is allowed to vary in section

4. Results are compared with truncated Fourier results of both MHD and neutral fluid theories. In section 5, we describe computer simulations of the discrete-vortex model and compare their numerical results with the analytical predictions. In section 6 we extend the model to three dimensions, with accompanying analysis and simulation results, and in section 7 we give a summary of the results and their implications.

II. Filamentary Representation of Two-Dimensional MHD

An MHD fluid is described in terms of two vector fields, the fluid velocity $\boldsymbol{v}(\boldsymbol{x},t)$ and the magnetic field $\boldsymbol{B}(\boldsymbol{x},t)$, in addition to two scalar fields, the fluid density ρ and pressure p. The pressure and density are usually related by an equation of state (we take $\rho = \text{const}$), and in a dissipationless system with incompressible flow, the vector fields obey

$$\begin{aligned} \frac{\partial \boldsymbol{v}}{\partial t} + (\boldsymbol{v}\cdot\nabla)\boldsymbol{v} &= -\frac{\boldsymbol{\nabla} p}{\rho} + \frac{(\boldsymbol{\nabla}\times\boldsymbol{B})\times\boldsymbol{B}}{4\pi\rho} \\ \frac{\partial \boldsymbol{B}}{\partial t} &= \boldsymbol{\nabla}\times(\boldsymbol{v}\times\boldsymbol{B}) \\ \boldsymbol{\nabla}\cdot\boldsymbol{v} = \boldsymbol{\nabla}\cdot\boldsymbol{B} &= 0. \end{aligned} \tag{1}$$

We will first treat the two dimensional case, i.e. all quantities are independent of some coordinate (say z), and $\boldsymbol{v}_z = \boldsymbol{B}_z = 0$. In this case, the vorticity, $\boldsymbol{\omega} \equiv \boldsymbol{\nabla}\times\boldsymbol{v} = \omega\hat{\boldsymbol{z}}$, and current $\boldsymbol{j} \equiv \boldsymbol{\nabla}\times\boldsymbol{B} = j\hat{\boldsymbol{z}}$ are scalars.

Long ago, Elsasser[20] pointed out that the MHD equations, (1), can be written in the form

$$\begin{aligned} \frac{\partial \boldsymbol{u}}{\partial t} + (\boldsymbol{w}\cdot\nabla)\boldsymbol{u} &= -\boldsymbol{\nabla}\eta \\ \frac{\partial \boldsymbol{w}}{\partial t} + (\boldsymbol{u}\cdot\nabla)\boldsymbol{w} &= -\boldsymbol{\nabla}\eta \\ \boldsymbol{\nabla}\cdot\boldsymbol{u} = \boldsymbol{\nabla}\cdot\boldsymbol{w} &= 0, \end{aligned} \tag{2}$$

where the new variables are

$$\boldsymbol{u} = \boldsymbol{v} + \boldsymbol{B} \quad , \quad \boldsymbol{w} = \boldsymbol{v} - \boldsymbol{B} \tag{3}$$

$$\eta = p + \frac{1}{2}\boldsymbol{B}^2. \tag{4}$$

The equations have been cast in dimensionless form, with the velocity measured in units of an arbitrary constant v_0, magnetic field measured in units of $B_0 = \sqrt{4\pi\rho v_0^2}$, and p in units of ρv_0^2. The quantity η is the fluid pressure plus the magnetic pressure. The ratio $2p/\boldsymbol{B}^2$, known as the "plasma beta," is a measure of the strength of the magnetic field relative to the pressure, and has important effects on the dynamical behavior of the system. Other parameters exist which similarly define such behavior regimes, such as the ratio of fluid kinetic energy to magnetic field energy. In our statistical theory, the difference between the kinetic and magnetic energies will emerge as a natural parameter upon which the expected states will depend.

Let us define functions Ω^s and A^s by

$$\begin{aligned} \Omega^u &= \nabla \times \boldsymbol{u} \quad , \quad \boldsymbol{u} = \nabla \times \boldsymbol{A}^u \\ \Omega^w &= \nabla \times \boldsymbol{w} \quad , \quad \boldsymbol{w} = \nabla \times \boldsymbol{A}^w. \end{aligned} \tag{5}$$

We will use a general species superscript s to indicate one of either u or w. In a neutral fluid, the vorticity is conservatively advected through the fluid. We seek an analogous result for our Ω^s's. Defining the differential operators

$$\begin{aligned} D^u \boldsymbol{V} &\equiv \partial_t \boldsymbol{V} - \nabla \times (\boldsymbol{u} \times \boldsymbol{V}) \\ D^w \boldsymbol{V} &\equiv \partial_t \boldsymbol{V} - \nabla \times (\boldsymbol{w} \times \boldsymbol{V}) \end{aligned} \tag{6}$$

one finds that the curl of the momentum equation becomes

$$D^w \Omega^u + D^u \Omega^w = 0, \tag{7}$$

while the curl of the induction equation may be written

$$D^w \boldsymbol{\Omega}^u - D^u \boldsymbol{\Omega}^w = 2\boldsymbol{S}, \tag{8}$$

in which there is a source term

$$\begin{aligned} \boldsymbol{S} &= \boldsymbol{\Omega}^w \times \boldsymbol{\Omega}^u \\ &\quad + [\boldsymbol{\Omega}^w \cdot \boldsymbol{\nabla} \boldsymbol{u} - \boldsymbol{\Omega}^u \cdot \boldsymbol{\nabla} \boldsymbol{w}] \\ &\quad + \frac{1}{2} \left[\nabla^2 (\boldsymbol{u} \times \boldsymbol{w}) - (\nabla^2 \boldsymbol{u}) \times \boldsymbol{w} - \boldsymbol{u} \times (\nabla^2 \boldsymbol{w}) \right]. \end{aligned} \tag{9}$$

We are interested in the possible forms $\boldsymbol{S}$ may take and particularly under what conditions $\boldsymbol{S}$ is small. In the two dimensional case, $\boldsymbol{\Omega} = \Omega \hat{\boldsymbol{z}}$, $\boldsymbol{A} = A\hat{\boldsymbol{z}}$, and $\boldsymbol{S} = S\hat{\boldsymbol{z}}$. We choose a gauge in which $\boldsymbol{\nabla} \cdot \boldsymbol{A} = 0$, so that $\Omega^s = -\nabla^2 A^s$. The equations of motion are therefore

$$\begin{aligned} \partial_t \Omega^u + \boldsymbol{w} \cdot \boldsymbol{\nabla} \Omega^u &= S \\ \partial_t \Omega^w + \boldsymbol{u} \cdot \boldsymbol{\nabla} \Omega^w &= -S. \end{aligned} \tag{10}$$

Most of the terms in $\boldsymbol{S}$ vanish identically, and what remains can be expressed in terms of the strain rates,

$$S = \sigma_1^u \sigma_2^w - \sigma_2^u \sigma_1^w, \tag{11}$$

where

$$\begin{aligned} \sigma_1^s &\equiv (\partial_x^2 - \partial_y^2) A^s, \\ \sigma_2^s &\equiv \partial_x \partial_y A^s, \\ \sigma^{s2} &\equiv \sigma_1^{s2} + \sigma_2^{s2}. \end{aligned} \tag{12}$$

An upper bound for the magnitude of S is therefore

$$|S| \leq \sigma^u \sigma^w. \tag{13}$$

For general flows, the rate of strain σ^s is neither larger nor smaller than the vorticity Ω^s. If, however, the fields consist of well-isolated sharply-peaked structures in Ω^s, then S is small. Consider, e. g., a filamentary structure, with

$$\Omega^u \begin{cases} \sim \alpha^u & r \leq a \\ = 0 & r > a \end{cases} \tag{14}$$

This has associated fields $u_\theta = \frac{1}{2}\alpha^u a^2/r$ and $\sigma^u = \alpha^u a^2/r^2$ for $r > a$. Imagine that we have many of these structures in u and w, separated by a typical distance d, with $d \gg a$. The evolution of a Ω^u structure will primarily be by conservative advection, at a rate $\boldsymbol{w}\cdot\boldsymbol{\nabla}\Omega^u$. In contrast, S gives a contribution on the order of $\alpha^u\alpha^w a^4/d^4$ in typical locations between the filaments, and is only of the order $\alpha^u\alpha^w a^2/d^2$ at the filamentary sites. Thus, S is smaller than advection by at least an order in a/d.

Let Ω^s take the form

$$\Omega^s = \sum_i \alpha_i^s \delta(\boldsymbol{x} - \boldsymbol{x}_i^s). \tag{15}$$

Eq. (10) is solved by the motion of the filaments if

$$\begin{aligned} \frac{d\boldsymbol{x}_i^u}{dt} = \boldsymbol{w}(\boldsymbol{x}_i^u) \quad &, \quad \frac{d\boldsymbol{x}_i^w}{dt} = \boldsymbol{u}(\boldsymbol{x}_i^w) \\ \sum_i \frac{d\alpha_i^u}{dt}\delta(\boldsymbol{x} - \boldsymbol{x}_i^u) \;&=\; -\sum_i \frac{d\alpha_i^w}{dt}\delta(\boldsymbol{x} - \boldsymbol{x}_i^u) = S(\boldsymbol{x}) \end{aligned} \tag{16}$$

The induction of current represented by the source term is manifested by a simultaneous increase in the strength of u-filaments and a decrease in the strength of w-filaments. Because the sum of delta functions in the second equation can never exactly equal a general smooth function S, this solution is not a "weak" solution of the MHD equations in the same sense that the point-vortex evolution in hydrodynamics is a solution of the Euler equations. The validity of eq. (16) relies either on the number density of filaments of each species being large or on S being small.

Unlike hydrodynamics, in which each vorticity filament simply moves in the total velocity field, the filaments of a highly intermittent two-dimensional plasma fall into two species. The

u-filaments move in the field of the w's, and the w-filaments move in the field of the u's. Also, unlike the point-vortex solution of Euler's equation, the filaments change their intensities even in the absence of diffusion, similar to the vortices of geostrophic fluid motion on a rotating sphere[21] or of plasma drift waves.[22] Since this change is slow for isolated filaments, we proceed first with a treatment that neglects this effect.

III. Filaments With Fixed Strengths

This section deals with the statistics of u-w filaments for which the source S is neglected, so that individual filament strengths do not change in time. Let us have N_u filaments of type u and N_w of type w, $N_u + N_w = N$. The u's will have strength $\pm\alpha^u$ and w's $\pm\alpha^w$, and the domain will be a periodic box in (x, y) with volume V. The potentials are given by

$$A^s(\boldsymbol{x}) = -\int G(\boldsymbol{x}|\boldsymbol{x}')\Omega^s(\boldsymbol{x}')d\boldsymbol{x}' = -\sum_{i\in s}\alpha^s G(\boldsymbol{x}|\boldsymbol{x}_i^s), \tag{17}$$

where G is the Green's function for Poisson's equation, $\nabla^2 G = \delta(\boldsymbol{x} - \boldsymbol{x}')$, with appropriate boundary conditions. In an infinite domain, $G(\boldsymbol{x}|\boldsymbol{x}') \propto \ln|\boldsymbol{x} - \boldsymbol{x}'|$.

The filaments move by

$$\begin{aligned}\frac{d\boldsymbol{x}_i^u}{dt} &= \boldsymbol{w}(\boldsymbol{x}_i^u) = \boldsymbol{\nabla}\times\hat{\boldsymbol{z}}A^w(\boldsymbol{x}_i^u)\\ \frac{d\boldsymbol{x}_i^w}{dt} &= \boldsymbol{u}(\boldsymbol{x}_i^w) = \boldsymbol{\nabla}\times\hat{\boldsymbol{z}}A^u(\boldsymbol{x}_i^w),\end{aligned} \tag{18}$$

so this system of filaments is Hamiltonian with conjugate variables that are the normal Cartesian coordinates $(\sqrt{|\alpha|}x_i, \sqrt{|\alpha|}y_i)$. The Hamiltonian is

$$H(\boldsymbol{x}_1, \ldots, \boldsymbol{x}_N) = -\sum_{i\in u}\sum_{j\in w}\alpha_i^u\alpha_j^w G(\boldsymbol{x}_i|\boldsymbol{x}_j), \tag{19}$$

which may also be written

$$H = \int A^u\Omega^w = \int \boldsymbol{u}\cdot\boldsymbol{w} = \int \boldsymbol{v}^2 - \boldsymbol{B}^2. \tag{20}$$

The physical meaning of the Hamiltonian can be understood as follows: The potential energy of a given vorticity distribution $\boldsymbol{\omega}$ in a velocity field that arises from a vector potential $\boldsymbol{A}^v$ is given by

$$E^v_{\rm int} = \int \boldsymbol{\omega} \cdot \boldsymbol{A}^v. \tag{21}$$

For a given current distribution in a magnetic potential field, on the other hand, the magnetic interaction energy differs in the sign,

$$E^B_{\rm int} = -\int \boldsymbol{j} \cdot \boldsymbol{A}^B. \tag{22}$$

This is because work must be done against the magneto-inductive force in order to maintain a given current distribution while bringing it in from far away. By ignoring the source term in (8), we are slowly transferring energy into and out of the system by counteracting the inductive force along the filament. As a consequence, instead of the total magnetic plus kinetic field energy remaining constant, the total interaction energy $\int \boldsymbol{v}^2 - \boldsymbol{B}^2$ is conserved.

An isolated u or w filament has $\boldsymbol{v}$ and $\boldsymbol{B}$ fields of equal magnitude, and therefore makes no contribution to H. A key difference between discrete-vortex and Fourier-mode models of neutral fluids is that a singular vortex filament has infinite self-energy. This energy is usually subtracted as a constant from the Hamiltonian, although the scaling of this constant with the system size must be treated carefully.[23, 24] In the Fourier description, the self-energy of structures do not appear explicitly, and cannot be subtracted out. Our filamentary MHD representation differs from the Fourier description in a similar way, except that the self-energy of filaments, being exactly zero when S is neglected, need not be subtracted away.

In addition to being an interaction energy, H is a parameter whose sign determines whether the fluid is kinetically or magnetically dominated; thus, it carries the same kind of information as the plasma beta. The sign of H can be changed by reversing the signs of either α^u or α^w. This transformation simply switches the fields $\boldsymbol{v}$ and $\boldsymbol{B}$.

A. Canonical Ensemble

Given a statistical system with Hamiltonian H, let $f(E)$ denote the probability that the Hamiltonian will take the value E. The probability for two systems with E_1 and E_2 is $f(E_1)f(E_2)$, but if these two systems are considered jointly as a single system, the probability must be $f(E_1 + E_2)$. Thus, f must take the form $f \propto e^{-E/T}$ for a constant parameter T, which is called the temperature. This is the classical canonical ensemble. In general, there will be one temperature for each invariant that the system possesses. The normalization factor for the probability density function f is known as the partition function, and plays a central role in statistical theories. In our fixed-strength u-w filament system, the partition function is

$$Z = \int e^{-H/T} \prod_{i,s} d\boldsymbol{x}_i^s. \tag{23}$$

The choice of coordinates in the above integral is important. Only coordinates $\{q_i\}$ for which the volume element $\prod_i dq_i$ is constant during the evolution of the system give meaningful results. This requirement on the coordinates is known as Liousville's theorem, and it is automatically satisfied if the coordinates are the conjugate variables of a Hamiltonian system, as in our case.

In order to actually evaluate the integral, however, another choice of coordinates may be more convenient. We will make a change of variables from the coordinates of the filaments to the Fourier components of the filament densities, defined as

$$\rho_s(\boldsymbol{k}) = \frac{1}{V} \sum_i \alpha_i^s e^{i\boldsymbol{k}\cdot\boldsymbol{x}_i^s}. \tag{24}$$

Strictly speaking, there should only be as many ρ's as there are filaments. Nevertheless, if we retain a large number of modes, we find that the Jacobian of the transformation $\{\boldsymbol{x}_i\} \to \{\rho(\boldsymbol{k})\}$ is, with error $\sim 1/N$,

$$J = V^N \prod_{k,s} \frac{V^2}{\pi N_s \alpha_s^2} e^{\frac{-V^2}{N_s \alpha^{s2}} |\rho_s|^2}. \tag{25}$$

This can be verified directly by checking explicitly that

$$\left\langle |\rho_s|^{2n} \right\rangle = \int |\rho_s|^{2n} \prod_i d\boldsymbol{x}_i = \int J|\rho_s|^{2n} \prod_{k,s} d\rho_s = n! \left(\frac{N_s \alpha^{s\,2}}{V^2} \right)^n, \tag{26}$$

while the odd moments are zero. This technique is known as the "random-phase approximation",[25] because small-scale correlations between the filament positions have been ignored in calculating eq. (26). In terms of the ρ's, the Hamiltonian is

$$H = 2V \sum_{k \neq 0} \frac{1}{k^2} \Re(\rho_u \rho_w^*) + \text{const.}, \tag{27}$$

in which $\Re$ denotes the real part.

The partition function turns out to be

$$Z = \prod_k \frac{k^2}{k^2 - \gamma^2/k^2}, \tag{28}$$

in which γ is the (negative) normalized inverse temperature

$$\gamma = -\frac{\sqrt{N_u N_w}\alpha^u \alpha^w}{VT}. \tag{29}$$

The expected spectra are

$$\begin{aligned} \left\langle |\rho_s|^2 \right\rangle &= \frac{N_s \alpha^{s\,2}}{V^2} \frac{k^2}{k^2 - \gamma^2/k^2}, \\ \langle \Re(\rho_u \rho_w^*) \rangle &= \frac{\sqrt{N_u N_w}\alpha^u \alpha^w}{V^2} \frac{\gamma}{k^2 - \gamma^2/k^2}. \end{aligned} \tag{30}$$

Ensemble-average spectra of usual fluid quantities can be calculated from these density spectra by the relations

$$\begin{aligned} \left\langle |\omega|^2 \right\rangle &= \frac{1}{4} \left\langle |\rho_u + \rho_w|^2 \right\rangle \\ \left\langle |j|^2 \right\rangle &= \frac{1}{4} \left\langle |\rho_u - \rho_w|^2 \right\rangle \\ \langle v \cdot B \rangle &= k^{-2} \frac{1}{2} \left(\left\langle |\rho_u|^2 \right\rangle - \left\langle |\rho_w|^2 \right\rangle \right). \end{aligned} \tag{31}$$

In particular, when $N_u = N_w$ and $\alpha^u = \alpha^w$, $\langle \boldsymbol{v} \cdot \boldsymbol{B} \rangle = 0$, and the $|\omega|^2$ and $|j|^2$ spectra are

$$\left\langle |\omega|^2 \right\rangle = \frac{N_s \alpha^{s\,2}}{2V^2} \frac{k^2}{k^2 - \gamma},$$
$$\left\langle |j|^2 \right\rangle = \frac{N_s \alpha^{s\,2}}{2V^2} \frac{k^2}{k^2 + \gamma}. \tag{32}$$

The Hamiltonian takes the expected value

$$\langle H \rangle = \sum_k \left\langle |v|^2 \right\rangle - \sum_k \left\langle |B|^2 \right\rangle = \gamma \frac{2V}{N_s \alpha_s^2} \sum_k \frac{1}{k^4} |\omega|^2 |j|^2, \tag{33}$$

and is of the same sign as γ, which is constrained to $|\gamma| < k_{\min}^2$ because $\langle |\omega|^2 \rangle$ and $\langle |j|^2 \rangle$ must be positive.

By comparison, Kraichnan's truncated Fourier analysis for neutral fluids,[26] based on the invariance of the kinetic energy and the enstrophy, gives an equilibrium spectrum for the vorticity

$$\left\langle |\omega|^2 \right\rangle = \frac{k^2}{\alpha k^2 + \beta}. \tag{34}$$

In the neutral fluid spectra, either α or β may be negative, within appropriate restrictions that keep $\langle |\omega|^2 \rangle$ positive. Obviously, $\gamma > 0$ MHD states correspond to $\alpha > 0$, $\beta < 0$ neutral fluid states. By choosing appropriate temperatures, the denominator may be made arbitrarily small, and any total energy may be attained. The energy will be contained predominantly at $k_{\min}$, which is an indication of large-scale structure in ω. If a system contains equal numbers of filaments of both signs, such a state must take the form of one large cluster of each sign of filament. When $\gamma < 0$ in the MHD system, the magnetic field shows structure of the same form, with large-scale current distributions.

B. A Review of Fourier Statistics of Ideal MHD

Fyfe, Joyce, and Montgomery[27] have presented a Fourier-mode-based statistical theory of 2-D MHD like that of Kraichnan's for hydrodynamics. The Fourier components of the vorticity and current can be shown to obey Liousville's theorem, and there are three quadratic

constants of the motion which survive the truncation of modes $k_{\min}^2 \leq k^2 \leq k_{\max}^2$. They are the total energy, the cross helicity, and the mean square potential,

$$\begin{aligned} E = \ \tfrac{1}{2}\int(\boldsymbol{v}^2 + \boldsymbol{B}^2) \ &= \frac{1}{2}\sum_{\boldsymbol{k}} \frac{1}{k^2}(|\omega(\boldsymbol{k})|^2 + |j(\boldsymbol{k})|^2), \\ P = \ \tfrac{1}{2}\int \boldsymbol{v}\cdot\boldsymbol{B} \ &= \frac{1}{2}\sum_{\boldsymbol{k}} \frac{1}{k^2}\omega(\boldsymbol{k})j(-\boldsymbol{k}), \\ A = \ \tfrac{1}{2}\int A_z^2 \ &= \frac{1}{2}\sum_{\boldsymbol{k}} \frac{1}{k^4}|j(\boldsymbol{k})|^2. \end{aligned} \tag{35}$$

It has not been shown that other such constants do not exist. The construction of the canonical distribution for these constants with the partition function,

$$Z = \int \exp(-\alpha E - \beta P - \gamma A), \tag{36}$$

gives a predicted spectral distribution

$$\begin{aligned} \left\langle |j|^2 \right\rangle &= \frac{1}{2}\frac{k^2}{\alpha - \beta^2/4\alpha + \gamma/k^2}, \\ \left\langle |\omega|^2 \right\rangle &= \frac{k^2}{2}\left(\frac{1}{\alpha} + \frac{\beta^2/4\alpha^2}{\alpha - \beta^2/4\alpha + \gamma/k^2}\right). \end{aligned} \tag{37}$$

In the particular case in which $\langle \boldsymbol{v}\cdot\boldsymbol{B}\rangle = 0$, β is zero, and the spectra for $\boldsymbol{v}$ and $\boldsymbol{B}$ are

$$\begin{aligned} \left\langle |j|^2 \right\rangle &= \frac{k^2}{\alpha + \gamma/k^2} \\ \left\langle |\omega|^2 \right\rangle &= \frac{k^2}{\alpha}. \end{aligned} \tag{38}$$

The current spectrum of (38) allows for a spectrum peaked at $k_{\min}$ when γ is negative. It can also be shown that

$$\sum_{\boldsymbol{k}} \left\langle |\boldsymbol{v}|^2 \right\rangle - \sum_{\boldsymbol{k}} \left\langle |\boldsymbol{B}|^2 \right\rangle = \gamma\frac{2A}{\alpha}. \tag{39}$$

Whenever the magnetic energy is greater than the kinetic energy, γ will be negative, and the magnetic field will exhibit large-scale structure. This is just the same criterion for magnetic structure that the filamentary representation predicted in the previous section. There is, however, no possibility in (38) for ω to exhibit large-scale structure; indeed, $\langle|\omega|^2\rangle$

is independent of γ. An interesting point is that the quantity $\int \boldsymbol{v}^2 - \boldsymbol{B}^2$ is not an invariant of the ideal MHD equations, but the sign of the expected value of this quantity still is the determining parameter for whether there will be large-scale magnetic structure or not. In the filamentary picture, this quantity is exactly conserved.

The ω^2 spectra from eq. (38) gives a kinetic energy spectrum $\langle k^{-2}|\omega|^2\rangle$ partitioned equally between the modes regardless of the parameters of the system, and even when the magnetic field is identically zero. The spectrum is the same as if one had ignored the effects of enstrophy in the derivation of (34); indeed one has ignored these effects, since enstrophy is not an invariant of MHD. Still, as the magnetic field vanishes, the invariants of the system change. The total energy becomes the kinetic energy normally, but the mean square magnetic potential (A) goes to zero. The enstrophy, meanwhile, changes at a rate proportional to the magnetic field strength. As the magnetic energy vanishes, the enstrophy should be included as an invariant in the calculations, but it is not clear how to do this in a truncated Fourier theory.

C. Microcanonical Ensemble

If a system is isolated, then the appropriate choice for a probability function $f(E)$ is simply a delta function, which gives the classical microcanonical ensemble. The microcanonical ensemble is most appropriate for comparison with numerical studies of initial value problems, since such systems are typically isolated. A system must be ergodic if time-averaged quantities are to approach ensemble-averaged quantities as $t \to \infty$, and while any Hamiltonian system with few enough degrees of freedom will be integrable and hence not ergodic, most systems tend towards ergodicity with increasing degrees of freedom. Small-N systems of neutral-fluid vortices have been shown to be not entirely ergodic,[28] although the non-ergodicity appears to be weak even for $N = 8$.[29]

To study the microcanonical ensemble, we use the techniques of Edwards and Taylor.[30]

The value of the Hamiltonian is specified to be E, and the analog of the partition function, the structure function, is

$$\Phi(E,V,N) = \int \delta(E-H) \prod_{i,s} d\boldsymbol{x}_i^s, \tag{40}$$

from which follows the entropy, temperature, and pressure:

$$S(E,V,N) = \ln \Phi \tag{41}$$

$$\frac{1}{T} = \left(\frac{\partial S}{\partial E}\right)_{V,N} \tag{42}$$

$$P = \left(\frac{\partial S}{\partial V}\right)\left(\frac{\partial S}{\partial E}\right)^{-1} \tag{43}$$

Because our phase variables are physical coordinates, Φ is bounded by the volume of our system. A general feature of systems with bounded phase space is states with negative temperatures,[31] which show increased order with higher energies.

Using the explicit representation of the delta function, and invoking the random-phase approximation once again, we calculate

$$\Phi = \frac{1}{2\pi} \int d\lambda J \prod_{k,s} d\rho_s e^{i\lambda[E - 8\pi V \sum_k \frac{1}{k^2} \Re(\rho_u \rho_w^*)]}, \tag{44}$$

in which the domain of the ρ_s's is the entire complex plane. These integrations are easily carried out, leaving only one integration over λ which we rescale to the dimensionless z, leaving

$$\tilde{\Phi} = \frac{1}{2\pi} \int dz e^{iz\tilde{E}} \prod_{n_x,n_y} \frac{1}{1+\frac{z^2}{\pi^2\kappa^4}}, \tag{45}$$

where

$$\tilde{\Phi} = \Phi \frac{\sqrt{N_u N_w}\alpha^u \alpha^w}{V^N},$$
$$\tilde{E} = \frac{E}{\sqrt{N_u N_w}\alpha^u \alpha^w}, \tag{46}$$

$\kappa^2 = n_x^2 + n_y^2$ is the dimensionless wavenumber, and $k^2 = \frac{4\pi^2}{V}\kappa^2$.

The product in the integrand runs over all $n_x, n_y \geq 0$ except $n_x = n_y = 0$, and the integral can be reduced to an infinite sum over residues, which occur along the imaginary axis at $z = \pm i\pi\kappa$. The general form for $\tilde{\Phi}$ is

$$\tilde{\Phi} = \sum_{n_x,n_y} P_{n-1}(|\tilde{E}|)e^{-\pi\kappa^2|\tilde{E}|}, \tag{47}$$

where P_{n-1} is a polynomial whose degree is one less than the degeneracy of the (n_x, n_y) mode, i.e., given (n_x, n_y), n is the number of distinct pairs (m_x, m_y) such that $n_x^2 + n_y^2 = m_x^2 + m_y^2$. In contrast to the hydrodynamical structure function,[30, 23] $\tilde{\Phi}$ is symmetric with respect to $\tilde{E}$, and differs from a Gaussian distribution in that it asymptotically approaches $e^{-\pi\kappa_{\min}|\tilde{E}|}$ as $\tilde{E} \to \pm\infty$. The hydrodynamical structure function also does not go into negative energies. Figure 1(a) shows the structure function of the hydrodynamical structure function, obtained from a numerical integration of the results of Ref..[30] Figure 1(b) shows the u-w structure function, $\tilde{\Phi}$, from a numerical integration of eq. (45), along with a Gaussian for comparison, both normalized and chosen to correspond at $\tilde{E} = 0$. Also shown are histogram data of $\tilde{E}$ from an ensemble of filament systems with fixed filament intensities and random filament positions. The small number of events in the tails of the distribution of $\tilde{E}$ causes some scatter in the data, but the data conform to the calculated structure function and clearly deviate from a Gaussian in the tail.

Ensemble averages are calculated similarly,

$$\langle F \rangle = \int F\delta(E - H) \prod_{i,s} d\boldsymbol{x}_i^s, \tag{48}$$

which give the filament density spectra,

$$\begin{aligned} \frac{\langle|\rho_u(m_x, m_y)|^2\rangle}{N_u\alpha^{u2}} &= \frac{\langle|\rho_w(m_x, m_y)|^2\rangle}{N_w\alpha^{w2}} \\ &= \frac{1}{V^2}\frac{1}{2\pi\tilde{\Phi}}\int dz e^{iz\tilde{E}} \frac{1}{1 + \frac{z^2}{\pi^2(m_x^2+m_y^2)^2}} \prod_{n_x,n_y} \frac{1}{1 + \frac{z^2}{\pi^2\kappa^4}}, \end{aligned} \tag{49}$$

and the cross-correlation spectrum,

$$\frac{\langle\rho_u(m_x, m_y)\rho_w^*(m_x, m_y)\rangle}{\sqrt{N_u N_w}\alpha^u\alpha^w}$$

$$= \frac{1}{V^2}\frac{1}{2\pi\tilde{\Phi}}\int dz \frac{-iz}{\pi\kappa^2} e^{iz\tilde{E}} \frac{1}{1+\frac{z^2}{\pi^2(m_x^2+m_y^2)^2}} \prod_{n_x,n_y} \frac{1}{1+\frac{z^2}{\pi^2\kappa^4}}. \tag{50}$$

While $\langle|\rho_u|^2\rangle$ and $\langle|\rho_w|^2\rangle$ are even in $\tilde{E}$, $\langle\rho_u\rho_w^*\rangle$ is odd. Both have a pronounced lowest-wavenumber component when $|\tilde{E}|$ is large.

We take $N_u = N_w$ and $\alpha^u = \alpha^w$, and evaluate (45), (49), and (50) numerically. Figure 2 shows $\langle\omega^2(\kappa^2)\rangle$ for $\tilde{E} = 2$. The spectrum of ω^2 always flattens out at large κ, and when $\tilde{E}$ is large, $\langle\omega^2(\kappa_{\min})\rangle$ grows proportional to $\tilde{E}$, while $\langle j^2(\kappa_{\min})\rangle$ approaches a constant value ≈ 0.26, which in fact is nearly reached by $\tilde{E} = 2$ (fig. 2). As mentioned before, changing the sign of $\tilde{E}$ interchanges the spectra of j^2 and ω^2, so a concentration of magnetic energy at long wavelengths is expected for $\tilde{E} \ll -1$, while the lowest mode of the ω^2 spectrum approaches a constant value.

The spectra predicted by the microcanonical ensemble are very similar in shape to those predicted for the canonical ensemble in the previous section. In general, the canonical and microcanonical ensembles are expected to coincide in the large degree of freedom limit, an our derivation of the spectra assumes large N through the use of the random-phase approximation. The most important features of these spectra are the long-wavelength peaks in either ω^2 or j^2, depending on the sign of $\tilde{E}$ (the value of the Hamiltonian). The strength of this peak scales as $\tilde{E}$, which goes like the total kinetic or magnetic energy in the small and large magnetic field limits, respectively.

D. Most Probable States

An interesting point raised in the case of neutral-fluid vortices,[32] which is also applicable here, is that there are two possible scalings of the energy with N, having to do with small-scale correlations between the filaments. When these correlations are neglected, the filaments interact only with the "mean field" of the other filaments. In this case, the random-phase approximation may be applied, and the energy scales $\propto N$. When small-scale correlations

are important, all pairs of filaments contribute to the energy, which scales $E \propto N^2$.

Without the random-phase approximation, direct calculation of spectra is difficult. It is still possible, however, to derive differential equations which describe the most-probable states of the system.[33] In our system of $N \equiv N_u + N_w$ filaments, let $n_+^u N_u$ of the u filaments have strength α^u, and $n_-^u N_u$ have strength $-\alpha^u$, and similarly for the w filaments. We define an N-Point probability function in the canonical ensemble,

$$P_N(\boldsymbol{r}_1^u, \ldots, \boldsymbol{r}_{n_+^u N_u}^u, \ldots, \boldsymbol{r}_{N_u}^u, \boldsymbol{r}_1^w \ldots, \boldsymbol{r}_{n_+^w N_w}^w, \ldots, \boldsymbol{r}_{N_w}^w) = e^{-H/T}/Z \tag{51}$$

which has been normalized such that

$$\int P_N d\boldsymbol{r}_1^u \ldots d\boldsymbol{r}_{N_w}^w = 1. \tag{52}$$

We define the single-filament probability densities of positive and negative filaments of both types

$$\begin{aligned} P_1^{u+}(\boldsymbol{r}) &= \int P_N \delta(\boldsymbol{r} - \boldsymbol{r}_1^u) d\boldsymbol{r}_1^u \ldots d\boldsymbol{r}_{N_w}^w, \\ P_1^{u-}(\boldsymbol{r}) &= \int P_N \delta(\boldsymbol{r} - \boldsymbol{r}_{n_+^u N_u + 1}^u) d\boldsymbol{r}_1^u \ldots d\boldsymbol{r}_{N_w}^w, \\ &\vdots \end{aligned} \tag{53}$$

which, once known, give the Ω^s fields by

$$\begin{aligned} \langle \Omega^s \rangle &= \int \sum_i \alpha_i^s \delta(\boldsymbol{r} - \boldsymbol{r}_i^s) P_N d\boldsymbol{r}_1^u \ldots d\boldsymbol{r}_{N_w}^w \\ &= N_s \alpha^s (n_+^s P_1^{s+} - n_-^s P_1^{s-}), \end{aligned} \tag{54}$$

and give the A^s's by

$$\begin{aligned} \langle A^s \rangle &= -\int \sum_i \alpha_i^s G(\boldsymbol{r}|\boldsymbol{r}_i^s) P_N d\boldsymbol{r}_1^u \ldots d\boldsymbol{r}_{N_w}^w \\ &= -N_s \alpha^s \left(n_+^s \int G(\boldsymbol{r}|\boldsymbol{r}') P_1^{s+}(\boldsymbol{r}') d\boldsymbol{r}' - n_-^s \int G(\boldsymbol{r}|\boldsymbol{r}') P_1^{s-}(\boldsymbol{r}') d\boldsymbol{r}' \right). \end{aligned} \tag{55}$$

Differentiating (53) with respect to $\boldsymbol{r}$ (and letting $\boldsymbol{\nabla}_1^u$ denote the gradient with respect to $\boldsymbol{r}_1^u$, etc.) gives

$$\begin{aligned}
\boldsymbol{\nabla} P_1^{u+} &= \int (\boldsymbol{\nabla}_1^u P_N)\delta(\boldsymbol{r}-\boldsymbol{r}_1^u)d\boldsymbol{r}_1^u \ldots d\boldsymbol{r}_{N_w}^w \\
&= \int -\frac{1}{T} P_N \boldsymbol{\nabla}_1^u H \delta(\boldsymbol{r}-\boldsymbol{r}_1^u)d\boldsymbol{r}_1^u \ldots d\boldsymbol{r}_{N_w}^w \\
&= \frac{\alpha^u}{T}\int \sum_j \alpha_j^w \boldsymbol{\nabla}_1^u G(\boldsymbol{r}_1^u|\boldsymbol{r}_j^w) P_N \delta(\boldsymbol{r}-\boldsymbol{r}_1^u)d\boldsymbol{r}_1^u \ldots d\boldsymbol{r}_{N_w}^w \\
&= n_+^w \frac{\alpha^u \alpha^w N_w}{T}\int \boldsymbol{\nabla}_1^u G(\boldsymbol{r}_1^u|\boldsymbol{r}_1^w) P_2^{u+w+}\delta(\boldsymbol{r}-\boldsymbol{r}_1^u)d\boldsymbol{r}_1^u d\boldsymbol{r}_1^w \\
&\quad -n_-^w \frac{\alpha^u \alpha^w N_w}{T}\int \boldsymbol{\nabla}_1^u G(\boldsymbol{r}_1^u|\boldsymbol{r}_{n_+^w N_w+1}^w) P_2^{u+w-}\delta(\boldsymbol{r}-\boldsymbol{r}_1^u)d\boldsymbol{r}_1^u d\boldsymbol{r}_{n_+^w N_w+1}^w, \qquad (56)
\end{aligned}$$

where we have introduced the two-point probability densities, P_2, defined as the integral of P_N over all but two of the $\boldsymbol{r}_i$. In order to close our system, we make the approximation that $P_2^{u+w-} = P_1^{u+}P_1^{w-}$, etc., and arrive at

$$\begin{aligned}
\boldsymbol{\nabla} P_1^{u+} &= \frac{\alpha^w \alpha^u N_w}{T} P_1^{u+}\int \boldsymbol{\nabla}' G(\boldsymbol{r},\boldsymbol{r}')\left(n_+^w P_1^{w+}(\boldsymbol{r}') - n_-^w P_1^{w-}(\boldsymbol{r}')\right). \\
&= -\frac{\alpha^u}{T} P_1^{u+}\boldsymbol{\nabla}\langle A^w\rangle . \qquad (57)
\end{aligned}$$

Similar equations can be obtained for the other probability densities, giving

$$P_1^{u\pm} = \text{const.} \times e^{\mp\frac{\alpha_u}{T}\langle A^w\rangle} \quad , \quad P_1^{w\pm} = \text{const.} \times e^{\mp\frac{\alpha_w}{T}\langle A^u\rangle}. \qquad (58)$$

By using eq. (54), we arrive at a differential equation for the expected fields A^u and A^w,

$$\begin{aligned}
\nabla^2\langle A^u\rangle &= C^{u+}e^{\frac{\alpha^u}{T}\langle A^w\rangle} - C^{u-}e^{-\frac{\alpha^u}{T}\langle A^w\rangle} \\
\nabla^2 A^w &= C^{w+}e^{\frac{\alpha^w}{T}\langle A^u\rangle} - C^{w-}e^{-\frac{\alpha^w}{T}\langle A^u\rangle}. \qquad (59)
\end{aligned}$$

In the case in which $n_+^s = n_-^s$, this becomes

$$\begin{aligned}
\nabla^2 A^u &= C^{u2}\sinh(\frac{\alpha^u}{T}A^w) \\
\nabla^2 A^w &= C^{w2}\sinh(\frac{\alpha^w}{T}A^u). \qquad (60)
\end{aligned}$$

In the zero magnetic field limit, $A^u \to A^w$, and eq. (60) becomes exactly the "sinh-poisson equation," which describes the most probable states of a neutral fluid.[35, 24] Typical solutions of this equation consist of two oppositely-signed vortices with a size of the order of the system volume,[34] whereas when $n_+^s \neq n_-^s$, the corresponding equation for the most probable states contain a single vortex of the dominant sign.

If we let $\alpha^u = \alpha^w = \alpha$, then from (60) follows

$$\int |\nabla(A^u + A^w)|^2 = -\frac{T}{\alpha}\int \frac{\alpha}{T}(A^u + A^w)(\sinh\frac{\alpha}{T}A^u + \sinh\frac{\alpha}{T}A^w)$$
$$\int |\nabla(A^u - A^w)|^2 = \frac{T}{\alpha}\int \frac{\alpha}{T}(A^u - A^w)(\sinh\frac{\alpha}{T}A^u - \sinh\frac{\alpha}{T}A^w). \qquad (61)$$

Because sinh is a monotonic function, the integrands in eq. (61) are all positive definite. This constrains the solutions of (60) to obey $A^u + A^w = 0$ if T is positive, or $A^u - A^w = 0$ if T is negative. In other words, there arise two possibilities for the most probable state: either $\boldsymbol{B} = 0$, with the stream function obeying the sinh-Poisson equation, or $\boldsymbol{v} = 0$, with the vector potential obeying the sinh-Poisson equation.

IV. Filaments With Variable Strengths

We expand our investigation to allow the filament strengths to change in time under the inductive force and calculate expected spectra for the canonical ensemble. The phase space now consists of both the filament positions $\{x_i^s, y_i^s\}$, and their intensities $\{\alpha_i^s\}$. While x_i^s and y_i^s still obey Hamilton's equation, there is no suitable conjugate variable for α_i^s. However, we will show that the system does satisfy Liousville's theorem, and thus may be subjected to a statistical description. The flow is conservative in phase space if and only if

$$\sum_{i,s}\frac{\partial\dot{\alpha}_i^s}{\partial\alpha_i^s} + \frac{\partial\dot{x}_i^s}{\partial x_i^s} + \frac{\partial\dot{y}_i^s}{\partial y_i^s} = 0. \qquad (62)$$

In fact, we can prove a detailed Liousville's theorem in which each term of eq. (62) is satisfied separately. The x and y equations of motion are the same as in the Hamiltonian case, so

$$\frac{\partial \dot{x}_i^s}{\partial x_i^s} + \frac{\partial \dot{y}_i^s}{\partial y_i^s} = 0 \tag{63}$$

as before. That the remaining term is zero is no more than the statement that a filament does not change strength under its own field. This follows from the form of S in eqs. (11) and (12). The strain rates σ_1^s and σ_2^s arising from any axisymmetric potential $A^s(r)$ give zero when integrated over any circular region centered on $r = 0$, and $\sigma^s(r \to 0) \to 0$ if $\Omega^s(r \to 0) \to$ const. The effects on the shape of a filament due to S or from the advective shear are not considered here.

The case in which the S is ignored has only one constant of the motion: the Hamiltonian $\int \boldsymbol{u} \cdot \boldsymbol{w}$. Even though the source term has only a small effect on the motions of individual filaments, the overall effect of neglecting the source is to cause the usual constants of total energy, cross-helicity, and mean square potential to be no longer conserved. When we restore the effects of S, we expect these quantities to again become invariant. For our purposes, it is most convenient to speak of the conserved quantities,

$$E^u = \frac{1}{2}\int u^2 = \frac{1}{2}\int v^2 + B^2 + \int \boldsymbol{v} \cdot \boldsymbol{B}, \tag{64}$$

and

$$E^w = \frac{1}{2}\int w^2 = \frac{1}{2}\int v^2 + B^2 - \int \boldsymbol{v} \cdot \boldsymbol{B}, \tag{65}$$

in addition to the mean squared magnetic potential,

$$A = \frac{1}{8}\int (A^u - A^w)^2. \tag{66}$$

In order to determine to what extent these quantities are preserved by the u-w filament system, we write the energy E^u in terms of filament quantities and the Green's function G.

$$E^u = \frac{1}{2}\sum_{i,j} \alpha_i^u \alpha_j^u G(\boldsymbol{x}_i^u | \boldsymbol{x}_j^u) = \frac{1}{2}\sum_i \alpha_i^u A^u(\boldsymbol{x}_i^u). \tag{67}$$

This energy changes in time as

$$\dot{E}^u = \sum_i \dot{\alpha}_i^u A^u(\boldsymbol{x}_i^u) + \sum_i \alpha_i^u \hat{\boldsymbol{z}} \cdot \boldsymbol{u}(\boldsymbol{x}_i^u) \times \boldsymbol{w}(\boldsymbol{x}_i^u), \tag{68}$$

with $\dot{\alpha}_i^u = S(\boldsymbol{x}_i^u)$. The sum over filaments is just a Monte-Carlo approximation of the corresponding continuous integral. If the filaments are approximately randomly distributed (as for an ergodic system), these approximations will become exact in the limit $N_u \to \infty$,

$$\lim_{N \to \infty} \dot{E}^u = \int S A^u + \int \Omega^u \boldsymbol{u} \times \boldsymbol{w}. \tag{69}$$

Since, in two dimensions,

$$\begin{aligned} \int S A^u &= \frac{1}{2} \int A^u \nabla^2 (\boldsymbol{u} \times \boldsymbol{w}) - \frac{1}{2} \int A^u (\nabla^2 \boldsymbol{u}) \times \boldsymbol{w} - \frac{1}{2} \int A^u \boldsymbol{u} \times (\nabla^2 \boldsymbol{w}) \\ &= -\frac{1}{2} \int \Omega^u \boldsymbol{u} \times \boldsymbol{w} + \frac{1}{2} \int \Omega^u \boldsymbol{w} \cdot \boldsymbol{\nabla} A^u - \frac{1}{2} \int \Omega^w \boldsymbol{u} \cdot \boldsymbol{\nabla} A^u \\ &= -\int \Omega^u \boldsymbol{u} \times \boldsymbol{w}, \end{aligned} \tag{70}$$

this energy is conserved in the continuous limit, even though it is not manifestly conserved exactly for finite N.

We will again use the random-phase approximation to evaluate the partition function in terms of filament densities ρ_s.

$$E^u = \sum_{ij} \alpha_i^u \alpha_j^u G(\boldsymbol{x}_i^u | \boldsymbol{x}_j^u) = \sum_k \frac{1}{k^2} |\rho_u|^2 + \sum_k \frac{1}{k^2} \sum_i \alpha_i^{u2} \tag{71}$$

$$E^w = \sum_{ij} \alpha_i^w \alpha_j^w G(\boldsymbol{x}_i^w | \boldsymbol{x}_j^w) = \sum_k \frac{1}{k^2} |\rho_w|^2 + \sum_k \frac{1}{k^2} \sum_i \alpha_i^{w2}, \tag{72}$$

$$A = \sum_k \frac{1}{k^4} |\rho_u|^2 + |\rho_w|^2 - 2\Re(\rho_u \rho_w^*) + \sum_k \frac{1}{k^4} \left[\sum_i \alpha_i^{u2} + \sum_i \alpha^{w2} \right]. \tag{73}$$

These expressions contain self-energy terms, $\sum_i \alpha^{s2}_i$. When filament strengths are constant, these terms may be subtracted off, but in our case, the α^s's vary, so these terms must be treated more carefully. The partition function is

$$Z = \int e^{-E^u/T^u - E^w/T^w - A/T^A} \prod_{i,s} d\boldsymbol{x}_i^s d\alpha_i^s. \tag{74}$$

When we change the variables of integration from $\boldsymbol{x}_i^s, \alpha_i^s$, to the Fourier components, $\rho_s(\boldsymbol{k})$ (defined as before), we must use the Jacobian for which

$$\begin{aligned}
&\exp\left\{-\sum_k\left[\frac{1}{T^u k^2}+\frac{1}{T^A k^4}\right]\sum_i \alpha_i^{u2}\right. \\
&\quad\left.-\sum_k\left[\frac{1}{T^w k^2}+\frac{1}{T^A k^4}\right]\sum_j \alpha_j^{w2}\right\}\prod_{i,s} d\boldsymbol{x}_i^s d\alpha_i^s \\
&= J\prod_{k,s} d\rho_s d\rho_s^*.
\end{aligned} \tag{75}$$

This Jacobian is again a Gaussian, as can be verified by checking that the moments are

$$\int |\rho_s|^{2n} = n!\left(\frac{N_s\left\langle\alpha^{s2}\right\rangle}{V^2}\right)^n \tag{76}$$

to leading order in N. All that differs from the case in which the filament strengths are fixed is the replacement of the constant α^{s2} by the expected value

$$\left\langle\alpha^{s2}\right\rangle = \int \alpha_i^{s2}\exp\left\{-\sum_k\left[\frac{1}{T^s k^2}+\frac{1}{T^A k^4}\right]\alpha_i^{s2}\right\} d\alpha_i^s. \tag{77}$$

Defining, as before, the normalized inverse temperatures,

$$\beta^s = \frac{N_s^2\left\langle\alpha^{s2}\right\rangle}{VT^s} \quad , \quad \beta^A = \frac{\sqrt{N_u N_w\left\langle\alpha^{u2}\right\rangle\left\langle\alpha^{w2}\right\rangle}}{VT^A}, \tag{78}$$

the partition function takes the form

$$Z = \prod_{\boldsymbol{k}}\left[\left(1+\beta^u k^{-2}+\beta^A k^{-4}\right)\left(1+\beta^w k^{-2}+\beta^A k^{-4}\right)-\beta^{A2}k^{-8}\right]^{-1}, \tag{79}$$

and the expected spectra are

$$\begin{aligned}
\left\langle|\rho_u|^2\right\rangle &= \frac{1+\beta^w k^{-2}+\beta^A k^{-4}}{\left(1+\beta^u k^{-2}+\beta^A k^{-4}\right)\left(1+\beta^w k^{-2}+\beta^A k^{-4}\right)-\beta^{A2}k^{-8}}, \\
\left\langle|\rho_w|^2\right\rangle &= \frac{1+\beta^u k^{-2}+\beta^A k^{-4}}{\left(1+\beta^u k^{-2}+\beta^A k^{-4}\right)\left(1+\beta^w k^{-2}+\beta^A k^{-4}\right)-\beta^{A2}k^{-8}}, \\
\langle\Re(\rho_u\rho_w^*)\rangle &= \frac{\beta^A k^{-4}}{1+\beta^{u}k^{-2}+\beta^A k^{-4}}\left\langle|\rho_u|^2\right\rangle, \\
&= \frac{\beta^A k^{-4}}{1+\beta^{w}k^{-2}+\beta^A k^{-4}}\left\langle|\rho_w|^2\right\rangle,
\end{aligned} \tag{80}$$

where eq. (31) may again be used to derive spectra for ω and j. Even in the regime $\langle \boldsymbol{v} \cdot \boldsymbol{B} \rangle = 0$, eqs. (80) display a great range of possible behaviors. Some limits are of particular interest. When β^a and β^s are both large, $\langle |\omega|^2 \rangle$ and $\langle |j|^2 \rangle$ approach the results of the truncated Fourier theory, eq. (38). Spectra from this regime are shown in figure 3. Taking $\beta^A \to \infty$ with β^s finite gives $\langle |j|^2 \rangle \to 0$ with $\langle |\omega|^2 \rangle$ taking the appropriate neutral fluid form, eq. (34). When β^A and β^s are both order unity, and $\beta^u = \beta^w = -\beta^A$, the spectra conform to those of the $S = 0$ theory, eq. (32), as shown in figure 4. Eq. (80), therefore, contains all the behaviors of the theories previously outlined. The current exhibits large-scale structure when the magnetic field is large, and as $\boldsymbol{B}$ goes to zero, the vorticity shows similar organization, in a manner consistent with neutral fluid statistical theories.

V. Simulations of Two-Dimensional MHD Filaments

Numerical calculations have become an indispensable tool for the understanding of fluid systems. Given the difficulty of creating systems with two-dimensional geometries in the laboratory, computer models have often had to serve as tests of analytical theories. In the case of neutral fluid turbulence, high-resolution codes have demonstrated a fluid's tendency to form coherent vortex structures,[7] an effect completely missed by Fourier-mode statistical theories. A code which models vortex structures explicitly, with appropriately chosen dynamics,[36–38] can reproduce the behavior of the primitive fluid equations quite specifically, giving insight into what are the important processes of turbulence. We present results from a code (which will be described in a later paper) which models the discrete-vortex system (16). While we do not give direct comparison with numerical modeling of the MHD equations, these results may at the least provide confirmation of the analytical predictions of the previous section. Specifically, we compare computed spectra from the numerical initial-value problems with the predictions for the microcanonical ensemble from the previous section.

We run the system on a 2-D grid of 32×32 points. First runs were made with filaments

intensities fixed ($S = 0$), with an average filament density of one per cell (1024 of each species). We load the filaments randomly into boxes distributed on the grid, and vary the size of the boxes to provide some control over the initial energy. Shown in figure 5 are u-filament positions for a run with $\alpha^u = \alpha^w = 1$ and $\tilde{E} \approx 75$, such that the magnetic energy is much less than the kinetic energy. While clumping of the filaments is only barely visible from physical-space phase-space plots, the contour plots of the magnetic potential and the stream function shown in figure 6 clearly demonstrate that while the magnetic field has no obvious structure, the velocity field has been organized into one large positive and one negative vortex. Figure 7 shows a similar run with $\tilde{E} \approx 150$. In this run, the initial boxes are small enough that they evolve initially into distinct clusters, which gradually merge until there is only a single clump.

When studying systems of filaments with both signs of intensity, the box-loading technique does not satisfactorily produce negative energies. In order to obtain starting configurations with a particular desired energy, we employ a Monte-Carlo procedure. The filaments are given random positions, and individual filament positions are proposed. If the proposed configuration has energy closer to the target energy than the present configuration, the proposal is accepted. When the energy falls within an accepted range of the target energy, the positions are saved and become the initial conditions of the dynamic simulation. The systems are thus well-randomized at the beginning of the simulation, and need not be run for so long a time to obtain acceptable statistics.

A time history of the value of H was studied for a variety of separate runs, with varying grid sizes and filament densities. The numerical algorithm conserves the Hamiltonian to within round-off error. Interestingly, the quantities, E^u, E^w, and A, which are strict invariants under the continuous MHD fluid equations, simply fluctuate about a constant value in this approximate system. Their time histories are shown in figure 8(a)–(c). There is no net degradation or increase in the total energy, cross-helicity or mean-squared potential, which

further supports the contention that a u-w filament system even in which the source S is ignored still serves as an acceptable statistical model for MHD turbulence.

Energies down to ~ 1 are still large enough to show structure, even though the clustering of filaments represented by this is not visible from phase-space plots. Figure 9 shows contour lines of the magnetic and velocity fields from a run with $\tilde{E} = 2$. Typical spectra at a single time-step and averaged through the simulation are shown in figure 10. The solid line is the theoretical spectrum from the micro-canonical ensemble, as calculated in the previous section. The time-averaged quantities seem to correspond well with the micro-canonical ensemble averages.

As mentioned before, reversing the sign of the Hamiltonian should simply interchange the fields $\boldsymbol{v}$ and $\boldsymbol{B}$. Shown in figure 11 are spectra for a simulation run with $\tilde{E} = -1$. The same correspondence with theory is shown, this time with the magnetic energy spectrum exhibiting long-wavelength structure. Finally, figure 12 shows the values of the lowest wavenumber modes, $\omega^2(k_{\min})$ and $j^2(k_{\min})$, as a function of $\tilde{E}$. The asymptotic behaviors $\langle \omega^2 \rangle \propto \tilde{E}$ and $\langle j^2 \rangle \to$ const. are clearly demonstrated.

A number of runs were also carried out with $S \neq 0$. The filament strengths change according to S, with a global correction added to ensure conservation of E^u and E^w. Results from a pair of such runs are presented in figure 13. Although unconstrained, the values of A and H do not systematically decay in these cases either. The spectrum flattens out for large κ, and displays long-wavelength behavior consistent with the theoretical predictions. Because the theory was performed for a canonical ensemble rather than a micro-canonical ensemble, we do not make a direct comparison, but the similarities with the graphs in figures 3 and 4 are notable.

VI. Filamentary Objects in Three Dimensional MHD Turbulence

Let us suppose, as we have for two-dimensional turbulence, that the velocity and magnetic fields tend to form isolated structures, and study the collective interactions of such structures. That is, let a turbulent MHD fluid be represented as a collection of isolated u-w current-vorticity distributions which are advected by each other and whose strengths change according to a magneto-inductive source. The general Biot-Savart-like expression for u and w fields due to a system of filaments is

$$\begin{aligned} \boldsymbol{u}(\boldsymbol{x},t) &= \sum_i \alpha_i^u \int \frac{\boldsymbol{x}-\boldsymbol{r}_i^u(s,t)}{|\boldsymbol{x}-\boldsymbol{r}_i^u(s,t)|^3} \times \boldsymbol{r}^{u\prime}{}_i ds, \\ \boldsymbol{w}(\boldsymbol{x},t) &= \sum_j \alpha_j^w \int \frac{\boldsymbol{x}-\boldsymbol{r}_j^w(s,t)}{|\boldsymbol{x}-\boldsymbol{r}_j^w(s,t)|^3} \times \boldsymbol{r}^{w\prime}{}_j ds, \end{aligned} \tag{81}$$

where $\boldsymbol{r}_i^s(s,t)$ is a curve in terms of a parameter s that determines the spatial location of the filaments, and $\boldsymbol{r}_i^{s\prime} = \partial \boldsymbol{r}_i^s/\partial s$. This approach has already been used for hydrodynamical vortex filament simulations.[39] Since this decomposition is still rather intractable, we describe the vortices in terms of a multipole expansion, i.e. as a sum over derivatives of the Green's function

$$\boldsymbol{A}^s(\boldsymbol{x},t) = \sum_{n=0}^{\infty} \frac{1}{n!} \boldsymbol{M}^{(n)}_{i_1,\ldots,i_n}(t) \frac{\partial^n}{\partial x_{i_1} \ldots \partial x_{i_n}} G(\boldsymbol{x}|\boldsymbol{x}^s(t)). \tag{82}$$

An arbitrary field can be represented by suitably chosen distributions of point particles possessing internal degrees of freedom (the multipole moments $\boldsymbol{M}$). The equations of motion of a u-vortex are solved by

$$\begin{aligned} \dot{\boldsymbol{x}}^u &= \boldsymbol{w}(\boldsymbol{x}^u) \\ \dot{\boldsymbol{M}}^{(n)}_{i_1,\ldots,i_n} - (\boldsymbol{M}^{(n)}_{i_1,\ldots,i_n} \cdot \nabla)\boldsymbol{w}(\boldsymbol{x}^u) &= \boldsymbol{S}, \end{aligned} \tag{83}$$

and similarly for w-filaments. The source term is unique only up to an additive gradient, because such a gradient added to the potentials does not actually change the fields. The

source term again represents the induction of current in the advecting vortices. We will neglect this effect, and take $\boldsymbol{S} = 0$.

In three dimensions, the lowest non-trivial multipole moment for a divergenceless field is a point dipole or vortex ring. A treatment in terms of point dipoles for hydrodynamical turbulence was considered in[40] and.[41] In hydrodynamics, one must cope with the problem that a vortex loop moves under its own influence at a speed that scales inversely with the loop size. The problem of infinitely speedy rings is not present in our system, however, since a loop does not self-interact. The ith component of the dipole moment is given in terms of the jth component of $M_k^{(1)}$ by $D_i = \epsilon_{ijk} M_{jk}^{(1)}$.

Our turbulent fluid is represented by the positions and dipole strengths of the vortices, i.e. by the $6N$ variables $\boldsymbol{D}_i^s$ and $\boldsymbol{x}_i^s$. Defining the dipole field as

$$\boldsymbol{D}^s(\boldsymbol{x}) \equiv \sum_i \boldsymbol{D}_i^s \delta(\boldsymbol{x} - \boldsymbol{x}_i^s), \tag{84}$$

the field arising from the dipoles is given by

$$\boldsymbol{u}(\boldsymbol{x}) = \boldsymbol{D}^u(\boldsymbol{x}) - \boldsymbol{\nabla} \int \boldsymbol{\nabla}' \cdot \boldsymbol{D}^u(\boldsymbol{x}') G(\boldsymbol{x}|\boldsymbol{x}') d\boldsymbol{x}', \tag{85}$$

and the dipole moments change according to

$$\dot{\boldsymbol{D}}_i^u = -\boldsymbol{\nabla}(\boldsymbol{D}_i^u \cdot \boldsymbol{w})|_{\boldsymbol{x}_i^u} \quad , \quad \dot{\boldsymbol{D}}_i^w = -\boldsymbol{\nabla}(\boldsymbol{D}_i^w \cdot \boldsymbol{u})|_{\boldsymbol{x}_i^w}. \tag{86}$$

The evolution of the dipoles can thus be described by a Hamiltonian,

$$\begin{aligned} &H(\boldsymbol{x}_1^u, \boldsymbol{D}_1^u, \ldots, \boldsymbol{x}_N^u, \boldsymbol{D}_N^u) \\ &\quad = \sum_{i \in u} \boldsymbol{D}_i^u \cdot \boldsymbol{w}(\boldsymbol{x}_i^u) = \sum_{j \in w} \boldsymbol{D}_j^w \cdot \boldsymbol{u}(\boldsymbol{x}_j^w), \end{aligned} \tag{87}$$

where the $\boldsymbol{x}$'s are conjugate to the $\boldsymbol{D}$'s such that

$$\dot{\boldsymbol{x}}_i = \frac{\partial H}{\partial \boldsymbol{D}_i} \quad , \quad \dot{\boldsymbol{D}}_i = -\frac{\partial H}{\partial \boldsymbol{x}_i}, \tag{88}$$

and $\boldsymbol{u}(\boldsymbol{x})$ and $\boldsymbol{w}(\boldsymbol{x})$ are given by eq. (85). As in two dimensions,

$$H = \int \boldsymbol{u} \cdot \boldsymbol{w} = \int v^2 - B^2. \tag{89}$$

A. Canonical Ensemble

As a simple model, let us take a system of N_u u-dipoles and N_w w-dipoles each of which may have any orientation, but with fixed magnitudes D^u and D^w. The average dipole field $\langle \boldsymbol{D} \rangle$, is zero if the dipoles are non-correlated, but will in general be non-zero. Let us adopt, furthermore, a mean-field approximation, in which

$$\boldsymbol{u} = \frac{N_u}{V} \langle \boldsymbol{D}^u \rangle \quad , \quad \boldsymbol{w} = \frac{N_w}{V} \langle \boldsymbol{D}^w \rangle . \tag{90}$$

Our task is to find $\langle \boldsymbol{D}^w \rangle$ for given $\langle \boldsymbol{D}^u \rangle$ and vice-versa. The partition function is

$$Z = \left[\int e^{\frac{-N_u}{VT} |\langle \mathbf{D}^u \rangle| D^w \cos\theta} 2\pi D^{w2} d\cos\theta \right]^{N_w} . \tag{91}$$

Letting $\boldsymbol{D}^w = D^w_{\|} \langle \boldsymbol{D}^u \rangle / |\langle \boldsymbol{D}^u \rangle| + \boldsymbol{D}^w_{\perp}$, it is clear by symmetry that

$$|\langle \boldsymbol{D}^w \rangle| = \left| \left\langle D^w_{\|} \right\rangle \right| . \tag{92}$$

This parallel component may be obtained directly from the partition function:

$$\left\langle D^w_{\|} \right\rangle = D^w F \left(\frac{N_u |\langle \boldsymbol{D}^u \rangle| D^w}{VT} \right) , \tag{93}$$

with

$$F(x) = \frac{1}{x} - \coth x . \tag{94}$$

An identical calculation in which $\langle \boldsymbol{D}^w \rangle$ is fixed gives

$$\left\langle D^u_{\|} \right\rangle = D^u F \left(\frac{N_w |\langle \boldsymbol{D}^w \rangle| D^u}{VT} \right) . \tag{95}$$

This result is similar to the expected orientation of a system of magnetic dipoles. In that case, the parallel component solves $D_{\|} = F(\beta D_{\|})$. When the temperature drops below the Curie point, this equation acquires a non-zero solution, and the dipoles align themselves. Our solution is of the form $D_{\|} = F(\beta_1 F(\beta_2 D_{\|}))$. There is likewise a critical temperature,

$$T_c = \frac{1}{3} D^u D^w \sqrt{N_u N_w}/V, \tag{96}$$

such that for $|T| < T_c$, non-trivial solutions exist. For T positive, the dipoles align themselves with u's anti-parallel to w's. This is the minimum energy state, because it aligns the magnetic moments, but cancels the kinetic energy that the dipoles carry. In this simplified model with the magnitude of D^s fixed, the phase-space is bounded, and negative T states also exist, with all dipoles aligned parallel. However, in the full description, the magnitude of D^s is unconstrained and the phase-space is unbounded. In this case, only positive T is allowable, so we expect that a physical system will only admit states in which u and w dipoles are anti-aligned, i.e., states with a mean magnetic field. This is in contrast to the $S = 0$ two-dimensional case, in which the phase space is always bounded and there is a $\boldsymbol{v} \leftrightarrow \boldsymbol{B}$ symmetry.

B. Numerical Study

We employ a numerical code (to be described in a later paper) to advance the system (83) for 4096 dipoles of each species in a 16^3 computational cube. Dipoles were placed on grid points, and given random orientations. From such uniform random initial conditions, the system always chose to evolve a net magnetic field by orienting the u-dipoles opposite that w-dipoles. Figure 14 shows the mean alignment angle, $\langle \cos\theta \rangle \equiv \left\langle \hat{\boldsymbol{D}}^u \right\rangle \cdot \left\langle \hat{\boldsymbol{D}}^w \right\rangle$, for three runs with differing random initial conditions. The angle approaches π, indicating the net alignment of u and w dipoles pointing in opposite directions.

A glance at eq. (83) shows that there is the potential for exponential growth of a dipole in a suitable field. Indeed, two dipoles aligned opposite each other will move directly away from each other, and the magnitude of the dipole moments will grow in time without limit. This produces some computational hazards once the dipoles have aligned themselves. To study the behavior of dipoles which begin aligned, we conduct numerical runs in which a dipole is allowed to change its position and orientation, but not its magnitude. These runs begin with u dipoles oriented randomly within a cone pointing in the $+\hat{\boldsymbol{z}}$ direction, w dipoles

similarly oriented around $-\hat{z}$. This configuration corresponds to a mean magnetic field in $+\hat{z}$ with no net motion of the fluid.

Figures 15 and 16 show the computational volume of these fixed-magnitude runs. The initial magnetic field is generally vertical. Plotted in this volume are surfaces on which $B^2 = 0.7B^2_{\max}$. Stronger fields are present within the volume defined by this surface. Initially, B^2 is within 30% of the maximum throughout nearly the entire computational volume. The general attraction between oppositely-aligned dipoles brings u and w dipoles together, and the magnetic field becomes more localized. Finally the magnetic field becomes dominantly concentrated into a vertical column. These structures live for a time and then decay away, although the exact mechanism for this decay is still unclear.

VII. Conclusions and Discussion

We have presented a filamentary model for MHD in which two species of filaments are advected in each other's field while changing strength according to a source term. When this source is neglected, the system is Hamiltonian. The Hamiltonian is equal to the *difference* between the (bulk, not thermal) kinetic energy and the magnetic energy, a parameter not unlike the usual plasma beta. The usual invariants are not conserved by the source-less Hamiltonian system, although numerical calculations show that they simply fluctuate about a mean value. When the Hamiltonian is large and positive, the velocity field exhibits structure at the system's longest wavelength. For a system with no net circulation (i.e., zero total vorticity into and out of the plane), this structure has the form of two oppositely-rotating vortices, while the magnetic field has no large-scale structure. Conversely, when the Hamiltonian is large and negative, the stream-function switches roles with the magnetic potential, and the magnetic field is organized into two large-scale magnetic islands, while the velocity field is unorganized. As the magnetic field is reduced in strength, the expected states approach those of hydrodynamical theory, something that is not true of truncated

Fourier theory. When the source term is included, the source-less equilibrium states can be demonstrated to be a high-temperature limit of the source-included system, while the low-temperature limit gives the Fourier equilibria.

In three dimensions, a mean-field statistical calculation of singular dipoles shows that a turbulent magnetic fluid possesses a statistically favorable state in which there is no net fluid velocity, but a mean magnetic field does arise. Simulations bear this out, showing cylindrical concentrations of magnetic field in the complete absence of any driving forces.

The presence of coherent structures has come to be recognized as one of the most important features of neutral turbulence. Structures have profound effects on the dynamics of turbulence, but are not well represented by truncated Fourier statistics. While point-vortex theories are also limited in how they can describe extended structures in real fluids, they can provide a useful starting point. The search for structures in MHD turbulence is only just beginning, but evidence of strong intermittency in plasmas has long been observed, and there is every reason to believe structures will play important roles in magnetic turbulence as well. In this paper, we have shown that a point-vortex discretization like that of hydrodynamics is possible in general for MHD.

Our model assumes structure at the smallest scale, but the theory predicts structure on a large scale. This "self-organization" of the system takes place in the absence of both external forcing and dissipation. Most conventional theories of structure formation are based on the energy flow in dissipative systems,[42] and our theory should include a mechanism for dissipation to be complete. Progress in this direction has been made for neutral fluids[37, 38] by formulating rules for vortex merger, which is the dominant dissipative mechanism once coherent structures have emerged.

The present results may have applications in several areas. In the solar atmosphere, for example, to the extent that vertical flux ropes in the photosphere are two-dimensional, the two-dimensional theory may explain the tendency of these ropes to group together in

granules, super-granules, and sun-spots without relying on convective motion. The three-dimensional theory may be applied to the formation of magnetic flux ropes which form in the strongly turbulent, high-beta plasma of the solar convection zone, and then are carried outward by the bouyancy force. That the formation of these filaments is energetically favorable has been argued by Parker,[43] and it agrees with our statement that such a state is expected on statistical grounds. Our simulations in three dimensions also strongly suggest that such structures occur naturally.

Perhaps a very intriguing application may be made to a recent calculation[44, 45] which shows that, based on the fluctuation-dissipation theorem, a thermal plasma yields zero-frequency magnetic fluctuations, i.e., magnetic fields which are not necessarily constant throughout space, but which persist in time. Here too, the field does not arise from any driving force, but is simply a natural feature of the fluctuations about equilibrium in a plasma. In the low-frequency limit, this kinetic description should coincide with our own fluid model, so it is encouraging that both predict such a spontaneous emergence of structure. It is also extremely attractive to consider this as a candidate for cosmological structure formation.[46]

Other applications somewhat farther removed are vortical behavior in superfluids[47, 48] and high T_c superconductivities.[49, 50] It is also believed that the major part of physical behavior of the quantum Hall effect is due to vortices,[51, 52] and even such exotic applications as cosmic strings[53, 54] and polymer dynamics[55] may await us. We hope to explore many of these possibilities in future work.

Acknowledgements

We are grateful to professor J. B. Taylor for his insight and discussions. This work was supported by the U. S. Department of Energy and the National Science Foundation.

References

[1]D. Montgomery, L. Turner, and G. Vahala, Phys. Fluids **21**, 757 (1978).

[2]J. Ambrosiano & G. Vahala, Phys. Fluids **24**, 2253 (1981).

[3]R. Kinney, T. Tajima, H. Irie, Phys. Fluids B **5**, 118 (1993).

[4]H. Tasso, Phys. Lett. A**120**, 464 (1987).

[5]A. Royer, J. Math. Phys. **25**, 2873 (1984).

[6]R. H. Kraichnan and D. Montgomery, Rep. Prog. Phys. **45**, 547 (1980).

[7]J. C. McWilliams, J. Fluid Mech. **146**, 21 (1984);
J. C. McWilliams, J. Fluid Mech. **219**, 361 (1990).

[8]M. Brachet, M. Meneguzzi, H. Politano, and P. L. Sulem, J. Fluid Mech. **194**, 333 (1988).

[9]J. C. McWilliams, Phys. Fluids A **2**, 547 (1990).

[10]A. Pouquet, J. Fluid Mech. **88**, 1 (1978)

[11]J. O. Stenflo, Solar Phys. **32**, 41 (1973).

[12]F. Yusef-Zadeh, in *The Center of the Galaxy* (Boston: Kluwer, 1988), p. 243

[13]*Physics of Magnetic Flux Ropes*, ed. C. T. Russell, E. R. Priest, and L. C. Lee (Washington D. C.: AGU, 1990)

[14]H. Zirin, *Astrophysics of the Sun* (Cambridge: Cambridge University Press, 1988)

[15]V. Angelopoulos, W. Baumjohann, C. F. Kennel, F. V. Coroniti, M. G. Kivelson, R. Pellat, R. J. Walker, H. Luhr, and G. Paschmann, J. Geophys. Res. **97**, 4027 (1992).

[16]R. Jha, P. K. Kaw, S. K. Mattoo, C. V. S. Rao, Y. C. Saxena, and ADITYA Team, Phys. Rev. Lett. **69**, 1375 (1992).

[17]S. Orszag and C. Tang, J. Fluid. Mech **90**, 129 (1979).

[18]W. H. Matthaeus and D. Montgomery, Ann. NY Acad. Sci. **357** 203 (1980).

[19]D. Biskamp and H. Welter, Phys. Fluids B **2**, 1787 (1990)

[20]W. M. Elsasser, Phys. Rev. **79**, 183 (1950).

[21]N. J. Zabusky & J. C. McWilliams, Phys. Fluids **25**, 2175 (1982).

[22]M. Kono & W. Horton, Phys. Fluids B **3**, 3255 (1991).

[23]S. E. Seyler, Jr., Phys. Fluids **19**, 1336 (1976).

[24]D. Montgomer and G. Joyce, Phys. Fluids **17**, 1139 (1974).

[25]J. B. Taylor, Phys. Lett. A**40**, 1 (1972).

[26]R. H. Kraichnan, Phys. Fluids **8**, 575 (1965);
R. H. Kraichnan, Phys. Fluids **10**, 1417 (1967);
R. H. Kraichnan, J. Fluid Mech. **67**, 155 (1975).

[27]D. Fyfe and D. Montgomery, J. Plasma Physics **16**, 181 (1976).
D. Fyfe, G. Joyce, and D. Montgomery, J. Plasma Physics **17**, 317 (1977).
D. Fyfe, D. Montgomery, and G. Joyce, J. Plasma Physics **17**, 369 (1977).

[28]K. M. Khanin, Physica **D4**, 261 (1982).

[29]J. B. Weiss and J. C. McWilliams, Phys. Fluids **A3**, 835 (1991).

[30]S. F. Edwards and J. B. Taylor, Proc. R. Soc. Lond. **336A**, 257 (1974).

[31]L. Onsager, Nuovo Cime. Suppl. **6** (9), 279 (1949).

[32]Y. B. Pointin and T. S. Lundgren, Phys. Fluids **19**, 1459 (1976).

[33]T. S. Lundgren and Y. B. Pointin, J. Stat. Phys. **17**, 323 (1977).

[34]T. S. Lundgren and Y. B. Pointin, Phys. Fluids **20**, 356 (1977).

[35]J. G. Joyce and D. Montgomery, J. Plasma Phys. **10**, 107 (1973).

[36]G. F. Carnevale, J. C. McWilliams, Y. Pomeau, J. B. Weiss, and W. R. Young, Phys. Rev. Lett. **66**, 2735 (1991).

[37]J. B. Weiss & J. C. McWilliams, Phys. Fluids A, in press.

[38]R. Benzi, M. Colella, M. Briscolini, and P. Santangelo, Phys. Fluids A **4**, 1036 (1992).

[39]A. Pumir and E. Siggia, Phys. Fluids **30** (6), 1606 (1987).

[40]S. G. Chefranov, Sov. Phys. JETP **66** (1), 85 (1987).

[41]P. H. Roberts, Mathematika **19**, 169 (1972).

[42]G Nicolis, I. Prigogine, *Self-organization in nonequilibrium systems: from dissipative structures to order through fluctuations* (New York: Wiley, 1977).

[43]E. N. Parker, Ap. J. **191**, 245 (1974).

[44]T. Tajima, S. Cable, K. Shibata, and R. M. Kulsrud, Ap. J. **390**, 309 (1992).

[45]S. Cable and T. Tajima, Phys. Rev. A **46**, 3413 (1992).

[46]T. Tajima, S. Cable, & R. M. Kulsrud, Phys. Fluids B **4**, 2338 (1992).

[47]H. Kuratsuji, Phys. Rev. Lett. **68**, 1746 (1992).

[48]K. W. Schwartz, Phys. Rev. Lett. **64**, 415 (1990); Phys. Rev. Lett. **64**, 1130 (1990).

[49]R. H. Koch *et al.*, Phys. Rev. Lett. **63**, 1511, (1989).

[50]V. Kalmeyer & R. B. Laughlin, Phys. Rev. Lett. **59**, 2095 (1987).

[51]R. B. Laughlin, Phys. Rev. Lett. **50**, 1395 (1983).

[52]R. E. Prange & S. M. Girvin, eds. *The Quantum Hall Effect* (New York: Springer, 1987).

[53]H. Câteau & S. Saito, Phys. Rev. Lett., **65**, 2487 (1990).

[54]T. Vachaspati & A. Vilenkin, Phys. Rev. Lett. **67**, 1057 (1991).

[55]N. Saito, K. Takahashi, & Y. Yunoki, J. Phys. Soc. Jpn. **22**, 219 (1967).

Figure Captions

Figure 1.

Structure functions for (a) the single-species hydrodynamical system, and (b) the u-w system. Solid lines are from theory, while points are histograms from random data samples. The dotted line in (b) is a Gaussian distribution, shown for comparison.

Figure 2.

Spectra of $\langle \omega^2 \rangle$ from the u-w micro-canonical ensemble. Positive energies give large-scale velocity field structure.

Figure 3.

Equilibrium spectra of the u-w filamentary system with source included. Shown is (a) $\beta^u = \beta^w = 20$, $\beta^A = 10$ and (b) $\beta^u = \beta^w = 20$, $\beta^A = -10$. This regime is the low-energy limit for which the spectra approach the Fourier theory's predictions.

Figure 4.

Spectra of ω and j for (a) $\beta^u = \beta^w = -1/2$, $\beta^A = 1$ and (b) $\beta^u = \beta^w = 0.8$, $\beta^A = -0.8$. This regime is the high-energy limit that mimics the behavior of the $S = 0$ approximation.

Figure 5.

Phase-space plot of u-filament positions for $\tilde{E} \approx 75$ (a) at $t = 0$ and (b) at $t = 50$. Clusters of w filaments exist in the same location as u-clusters.

Figure 6.

Contours of (a) A_z and (b) Ψ for the final state of the run in the previous figure.

Figure 7.

Filament positions from a run with $\tilde{E} \approx 150$. Positions at $t = 0$ are shown in (a). Large clusters of filaments form by $t = 20$ in (b), eventually merging to a single clump near $t = 50$, as shown in (c).

Figure 8.

Time histories of (a) E^u, (b) E^w, and (c) A during a $S = 0$ run with $\tilde{E} = 2$.

Figure 9.

A_z and Ψ contours at $t = 70$ during $\tilde{E} = 2$ run.

Figure 10.

Spectra from a $\tilde{E} = 2$ run, showing (a) instantaneous vorticity spectrum, (b) instantaneous current spectrum, and (c) current and vorticity spectra averaged over the entire run of 2000 time steps ($t = 60$–70).

Figure 11.

Spectra from a $\tilde{E} = -1$ run, with format same as previous figure.

Figure 12.

Values of the minimum k mode of ω^2 and j^2 from a series of simulations, compared with theory.

Figure 13.

Spectra from (a) a velocity-dominated run, and (b) a magnetically-dominated run, in which diffusion has been compensated for. Spectra show shape and asymptotic behavior consistent with theory.

Figure 14.

Time history of mean alignment angle between u and w fields for three separate runs with different random initial conditions.

Figure 15.

Surfaces of constant B^2 for fixed dipole magnitude run in which the energy per dipole is .64 (a) at $t = 0$ and (b) at $t = 3$, as the field begins to organize.

Figure 16.

Continuation of the run from the previous figure, showing organization of magnetic field into flux tubes at times (a) $t = 6.0$ and (b) $t = 13.5$.

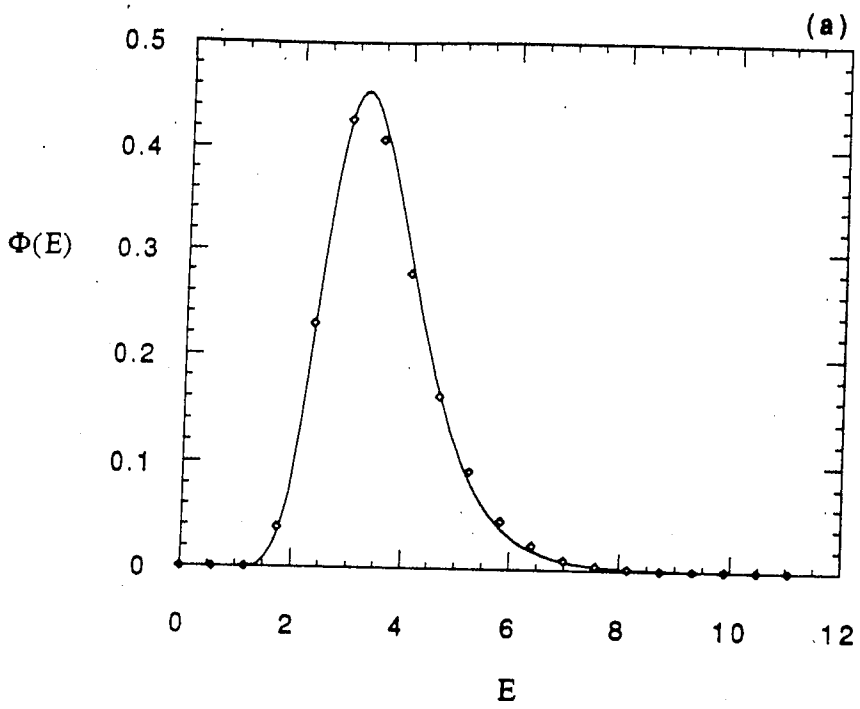

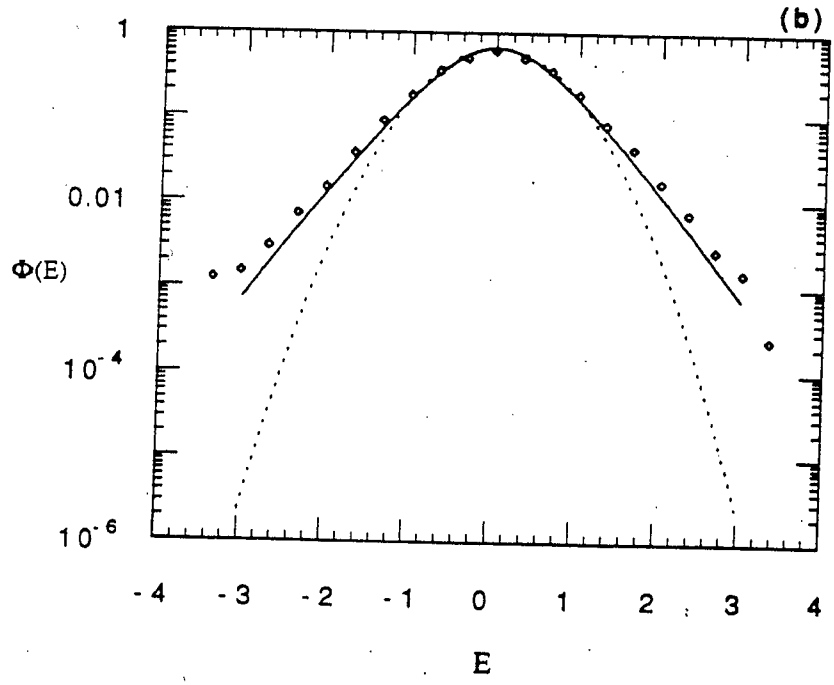

Fig 1

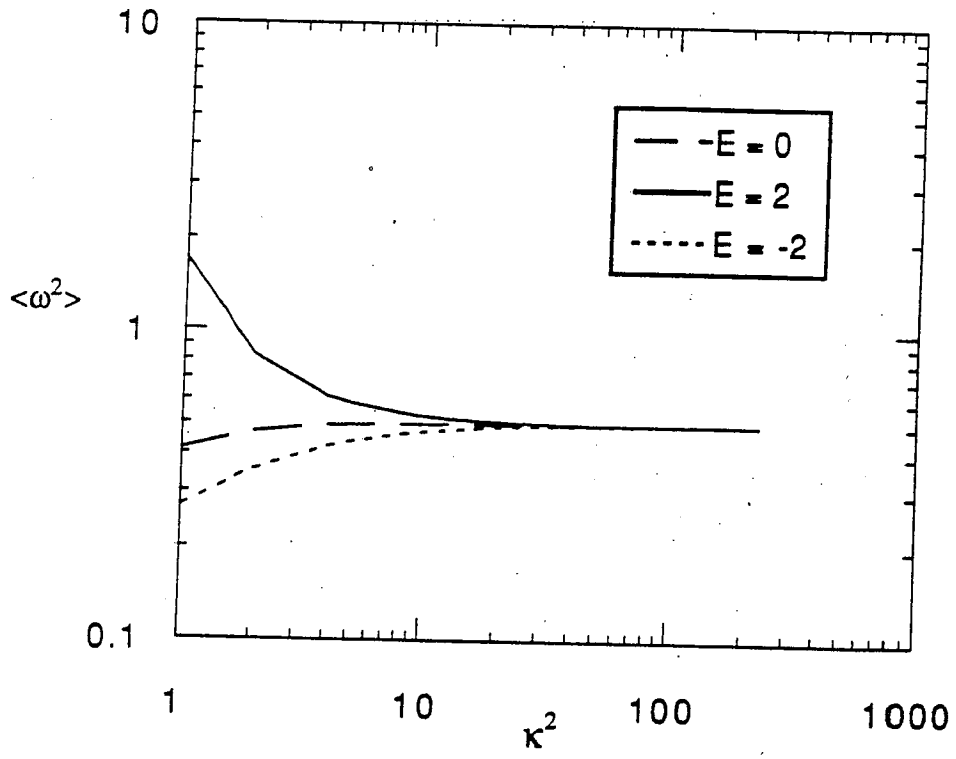

Fig 2

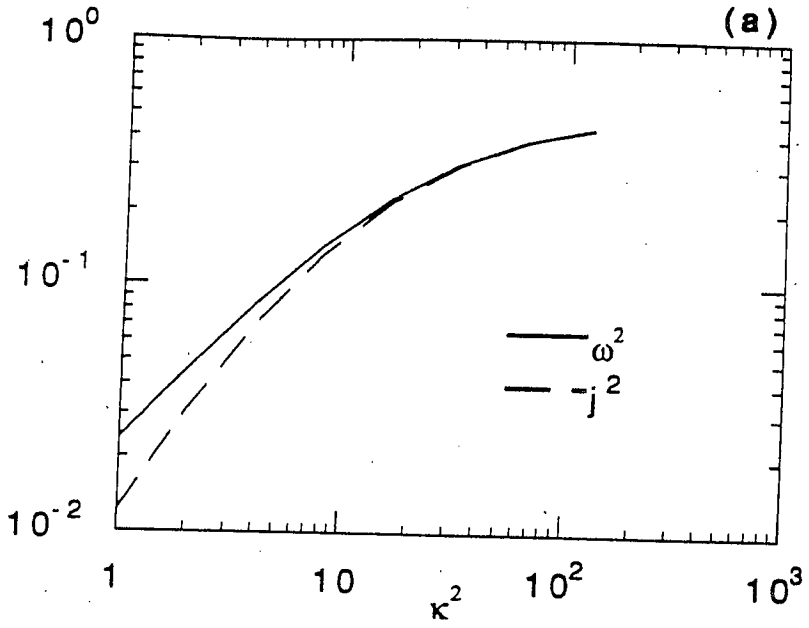
(a)
10^0
10^{-1}
10^{-2}
1
10
10^2
10^3
κ^2
ω^2
$-j^2$

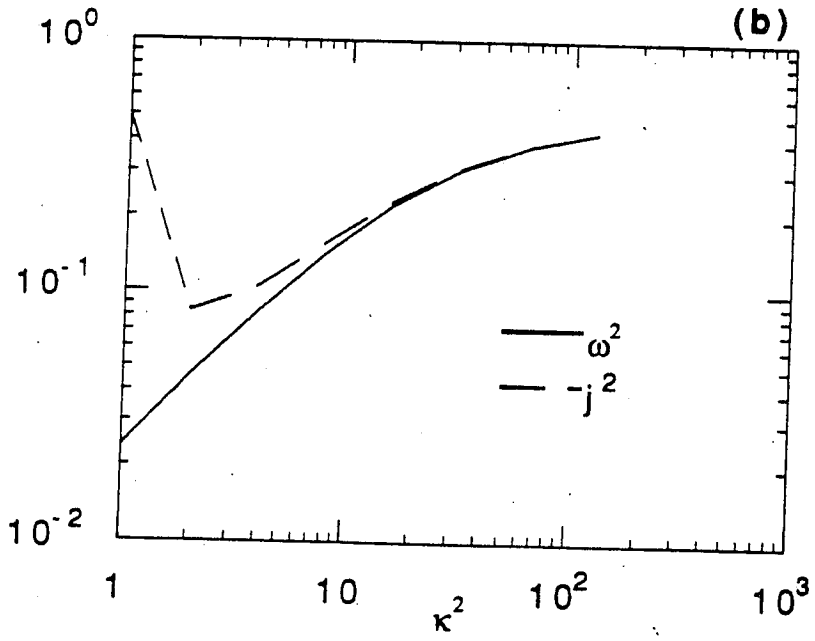
(b)
10^0
10^{-1}
10^{-2}
1
10
10^2
10^3
κ^2
ω^2
$-j^2$

Fig 3

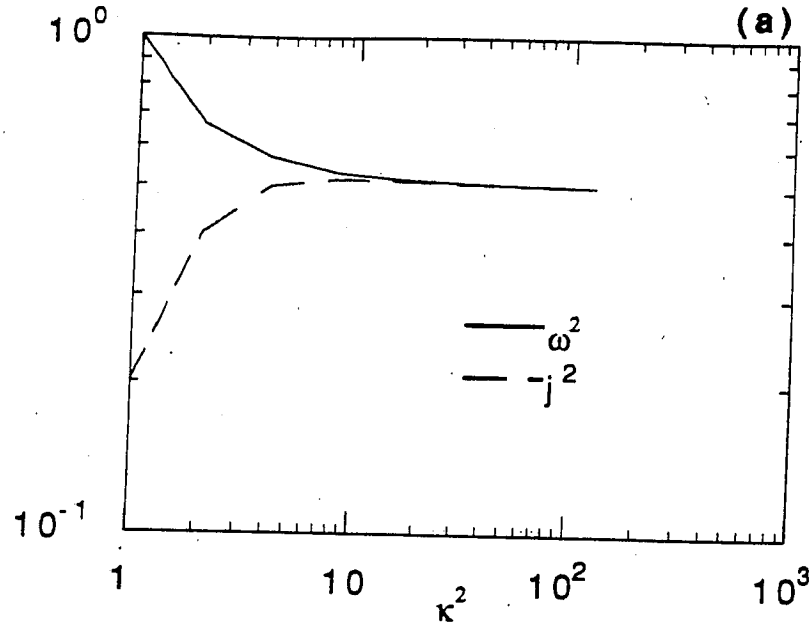
(a)
10^0
10^{-1}
1
10
10^2
10^3
κ^2
ω^2
$-j^2$

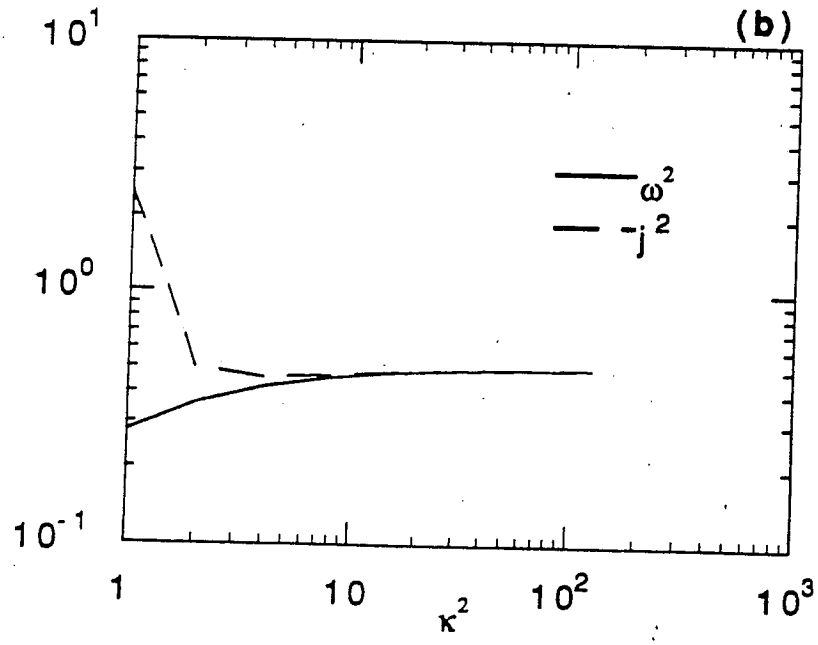
(b)
10^1
10^0
10^{-1}
1
10
10^2
10^3
κ^2
ω^2
$-j^2$

Fig 4

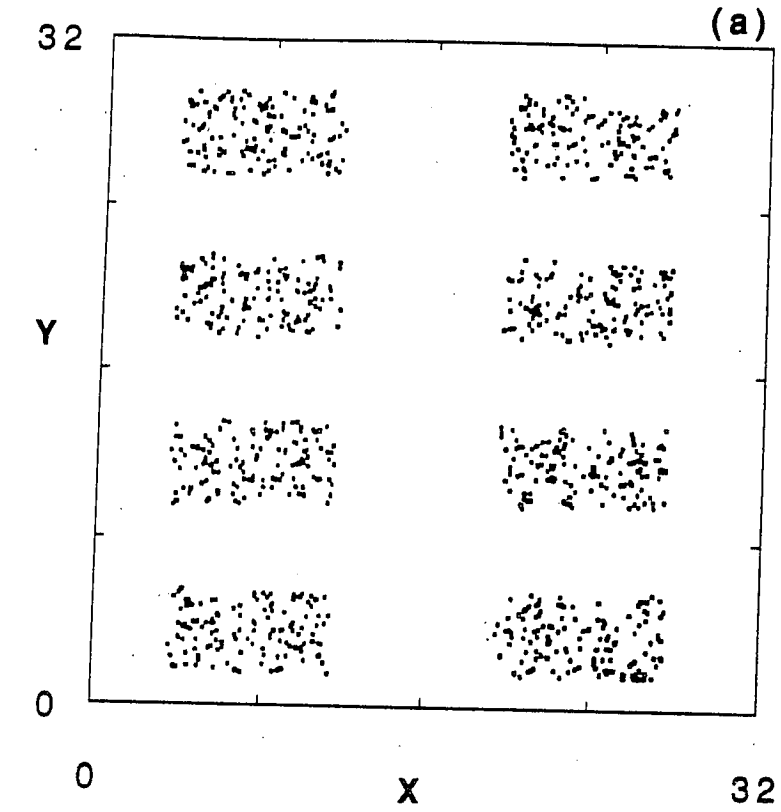

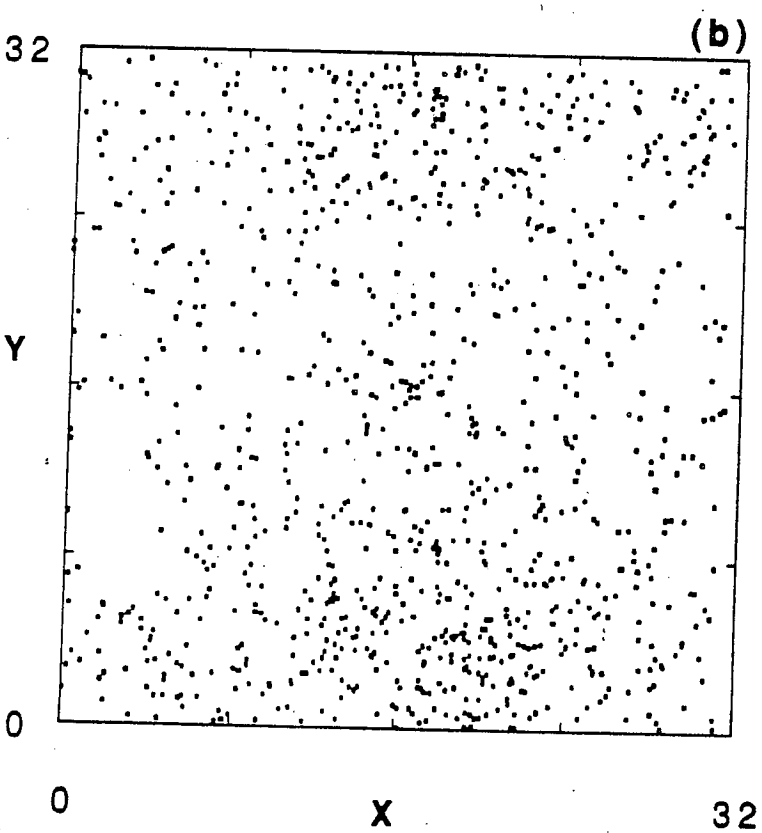

Fig 5

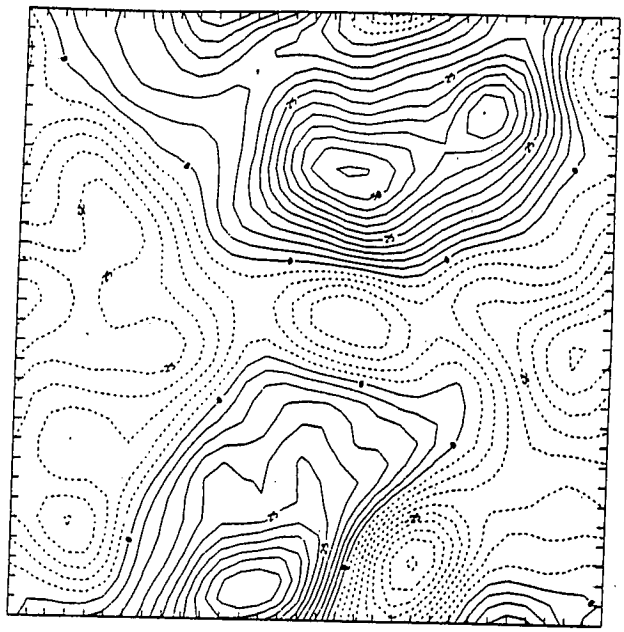

CONTOUR FROM -45 TO 55 BY 5

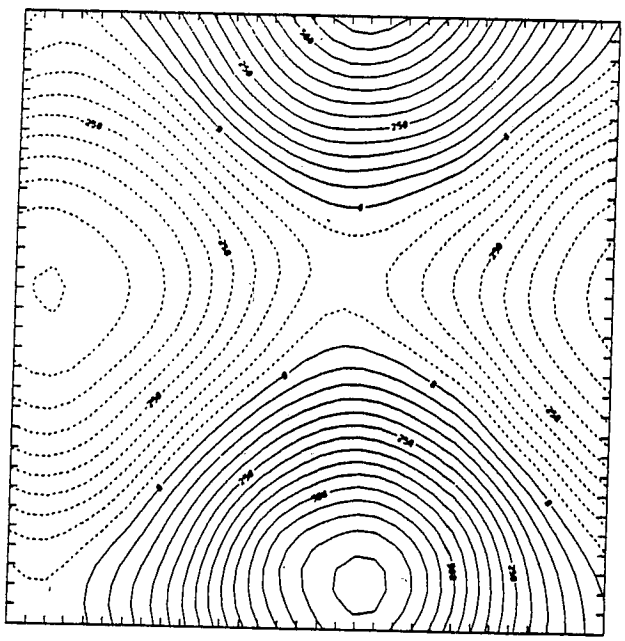

CONTOUR FROM -500 TO 700 BY 50

Fig 6

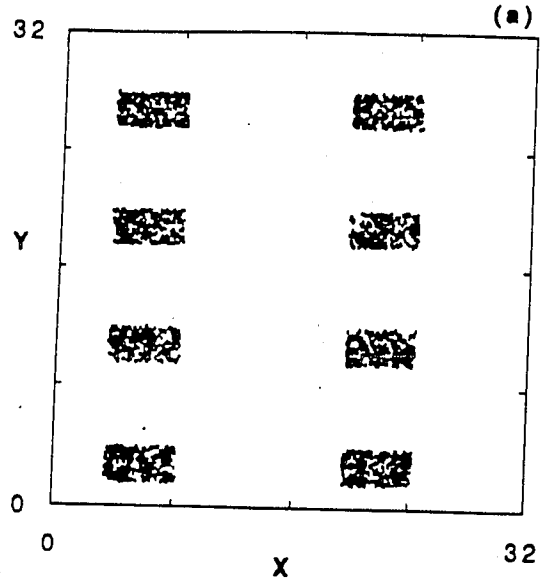

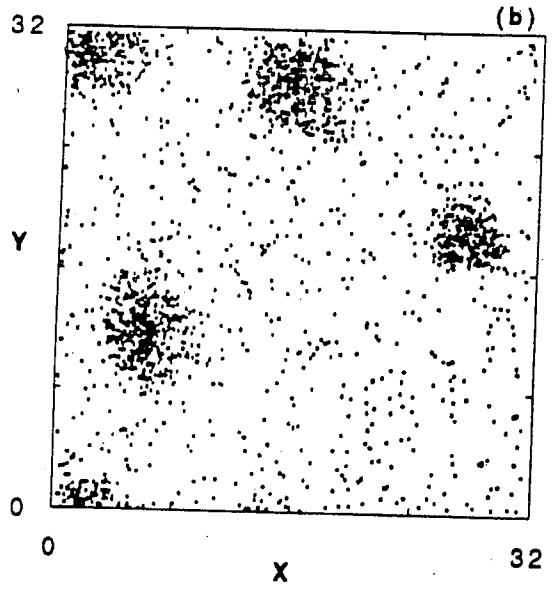

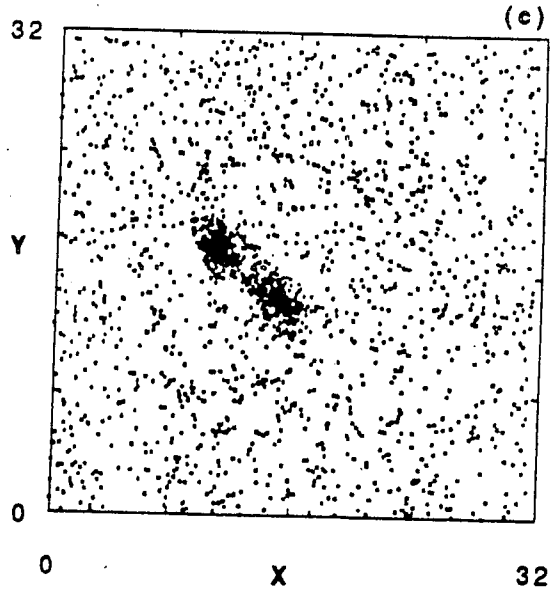

Fig 7

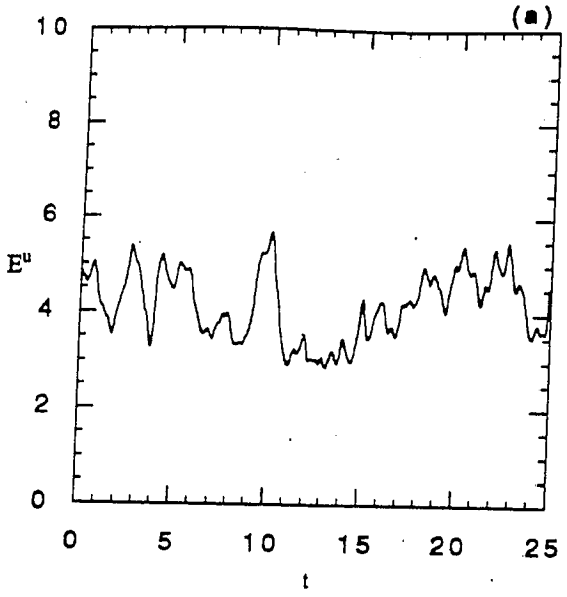
(a)
10
8
6
4
2
0
E^u
0
5
10
15
20
25
t

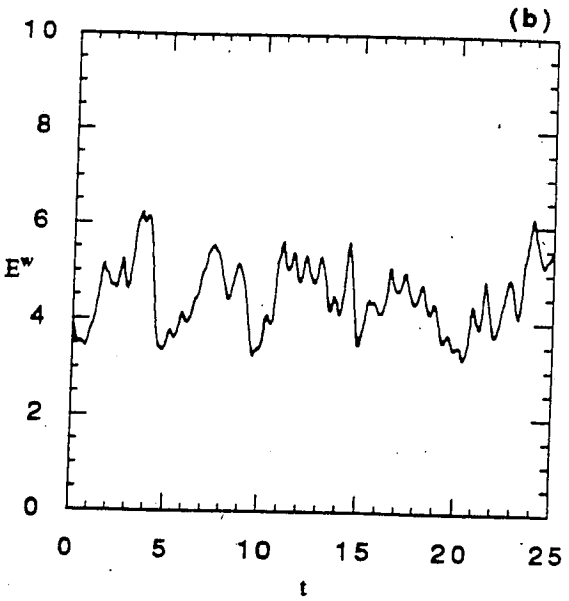
(b)
10
8
6
4
2
0
E^w
0
5
10
15
20
25
t

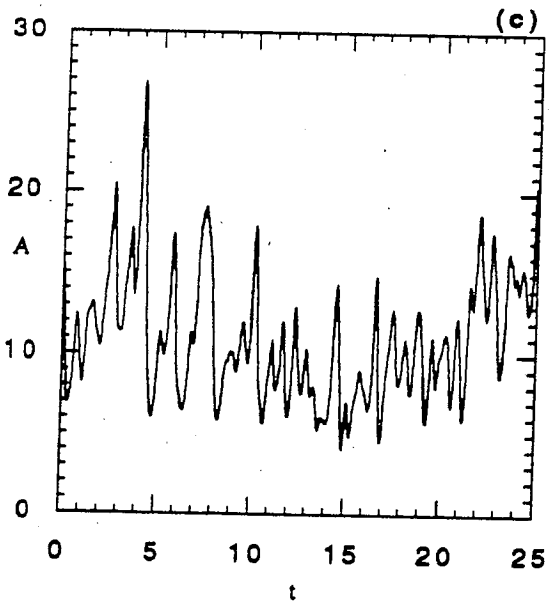
(c)
30
20
10
0
A
0
5
10
15
20
25
t

Fig 8

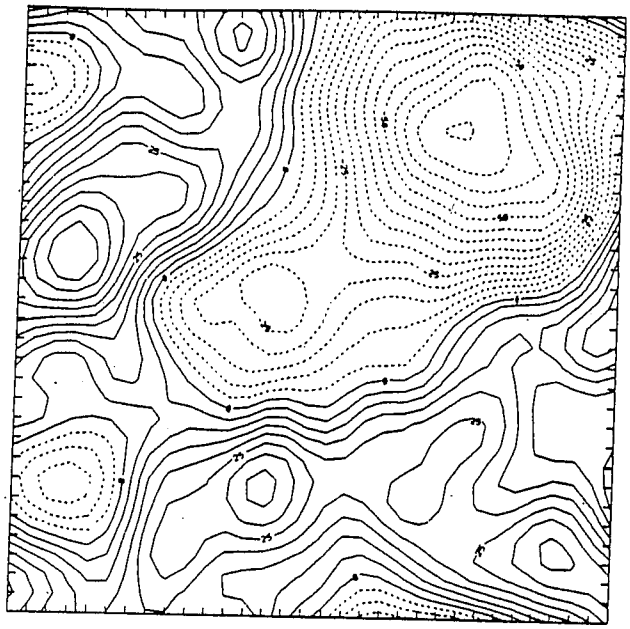

CONTOUR FROM -70 TO 45 BY 5

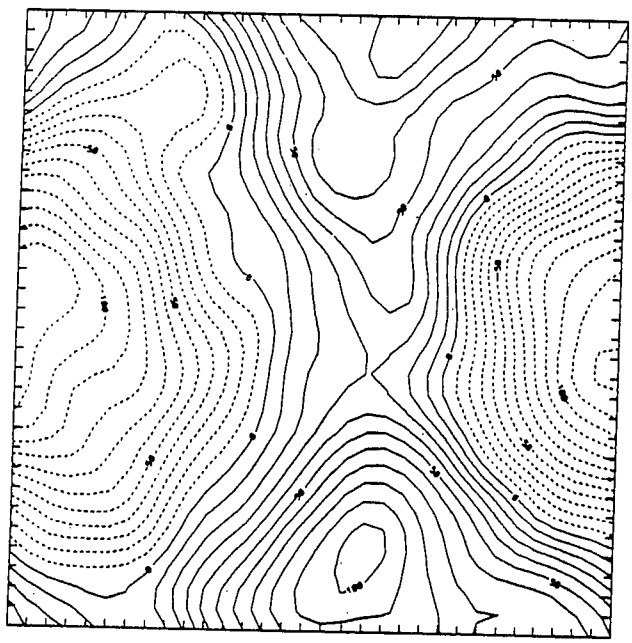

CONTOUR FROM -120 TO 100 BY 10

Fig 9

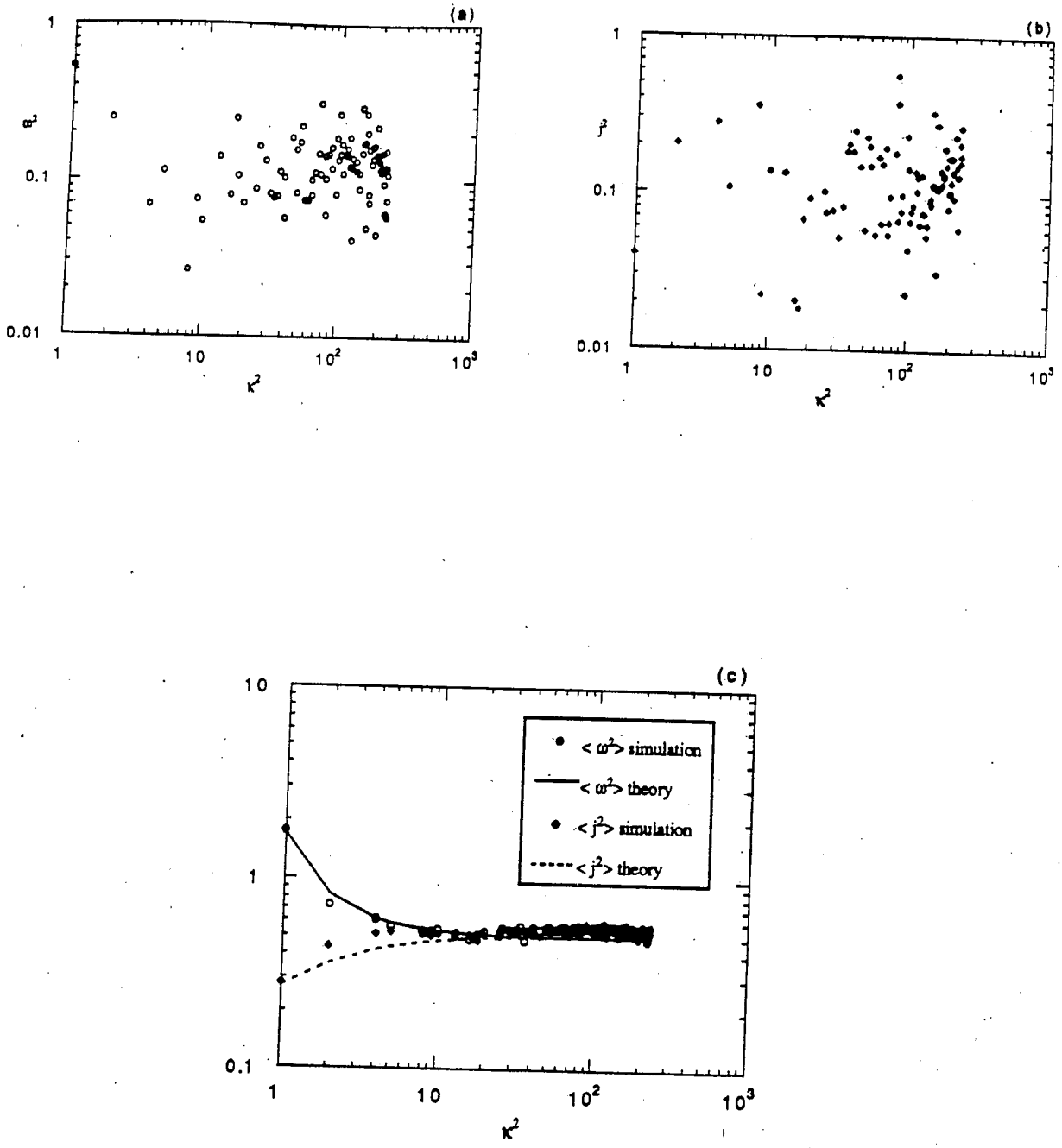
(a)
(b)
(c)
1
0.1
0.01
10
10^2
10^3
κ^2
ω^2
j^2
$< \omega^2 >$ simulation
$< \omega^2 >$ theory
$< j^2 >$ simulation
$< j^2 >$ theory

Fig 10

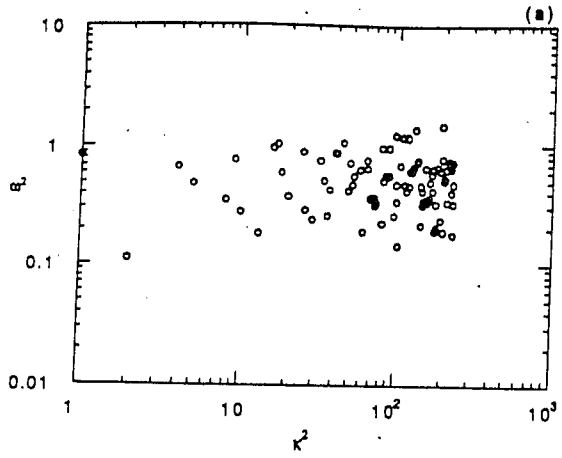
(a)
10
1
0.1
0.01
ω^2
1
10
10^2
10^3
κ^2

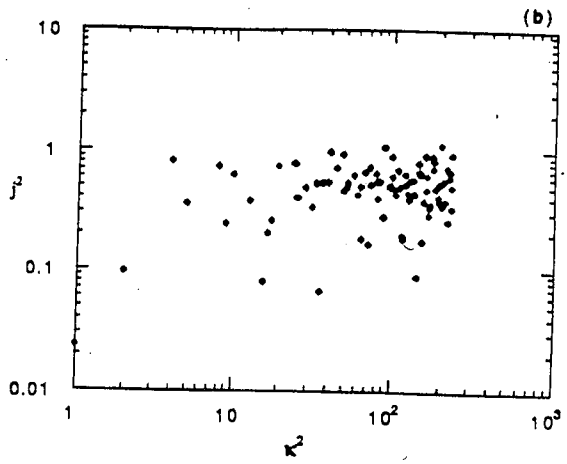
(b)
10
1
0.1
0.01
j^2
1
10
10^2
10^3
κ^2

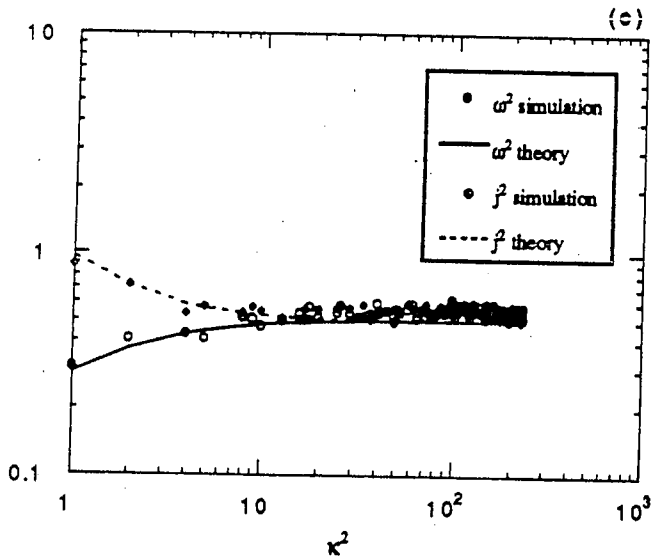
(c)
10
1
0.1
ω^2 simulation
ω^2 theory
j^2 simulation
j^2 theory
1
10
10^2
10^3
κ^2

Fig 11

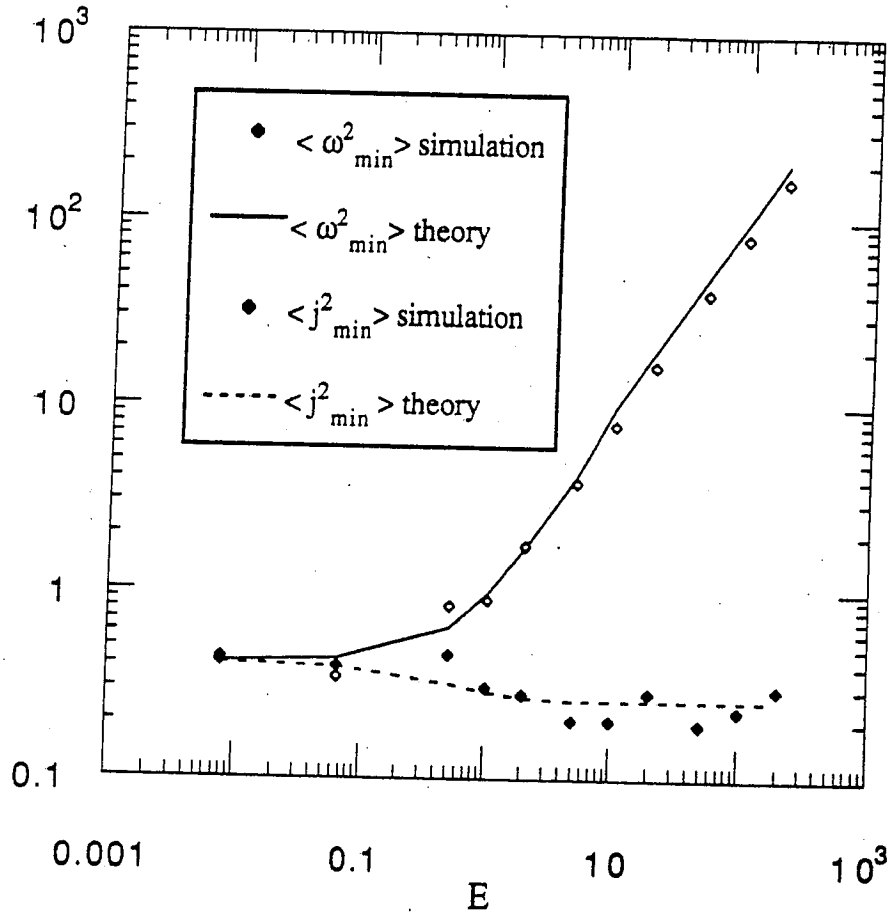
10^3
10^2
10
1
0.1
0.001
0.1
10
10^3
E
$< \omega^2_{min} >$ simulation
$< \omega^2_{min} >$ theory
$< j^2_{min} >$ simulation
$< j^2_{min} >$ theory

Fig 12

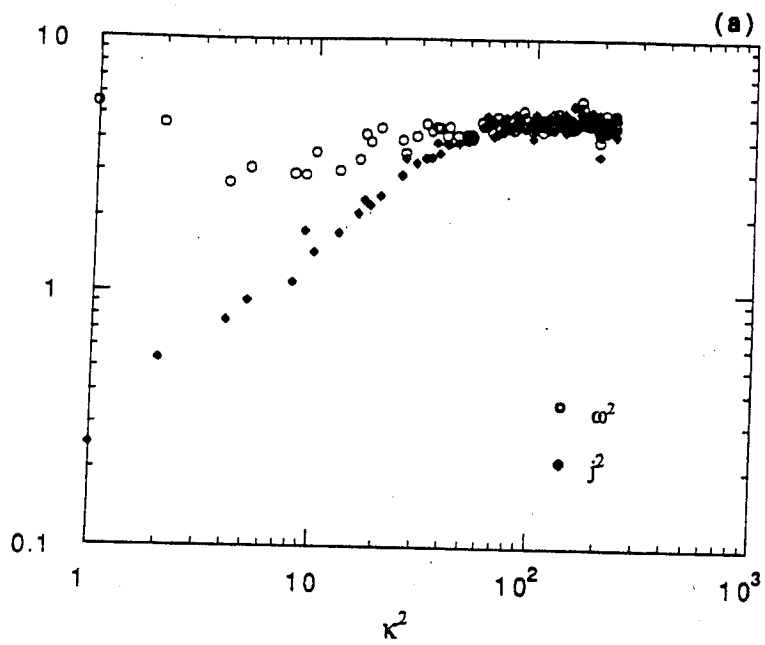
(a)
10
1
0.1
1
10
10^2
10^3
κ^2
ω^2
j^2

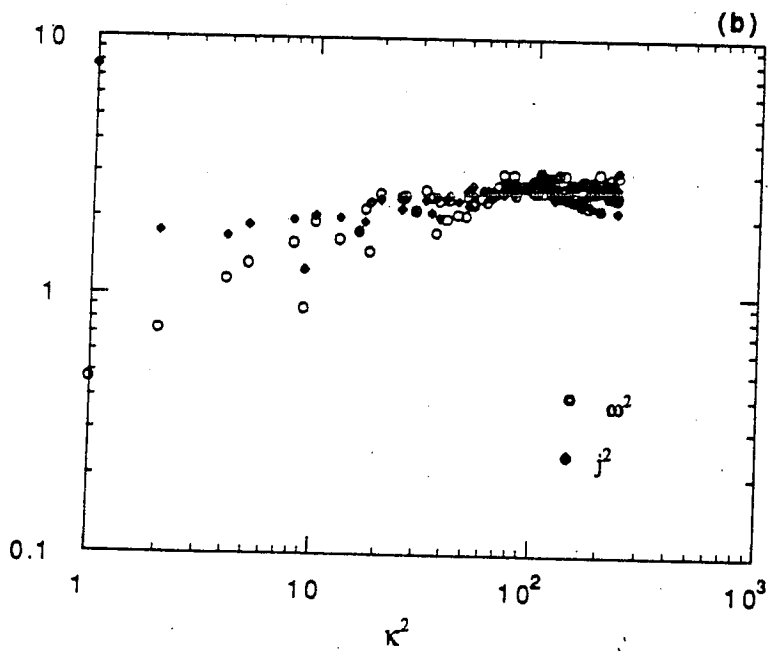
(b)
10
1
0.1
1
10
10^2
10^3
κ^2
ω^2
j^2

Fig 13

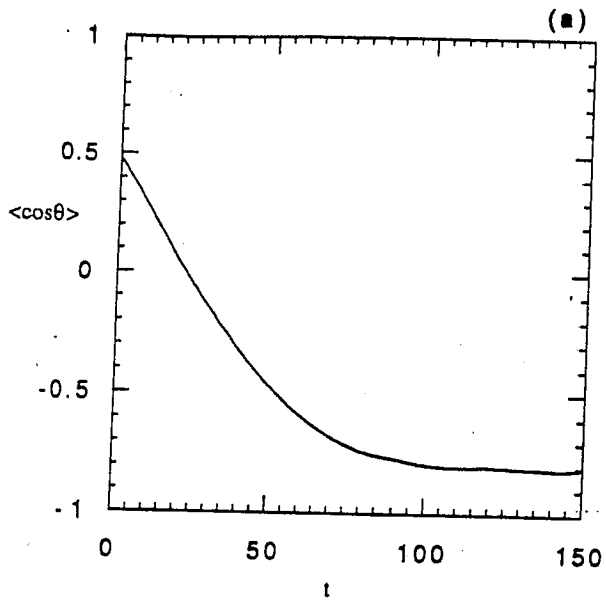
(a)
1
0.5
<cosθ>
0
-0.5
-1
0
50
100
150
t

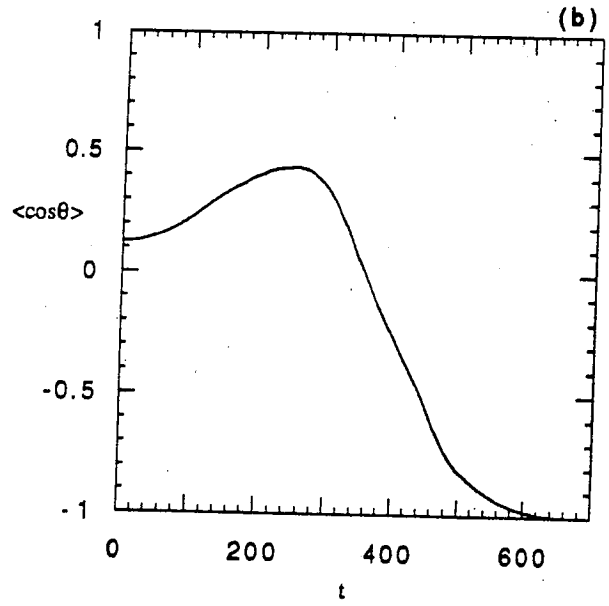
(b)
1
0.5
<cosθ>
0
-0.5
-1
0
200
400
600
t

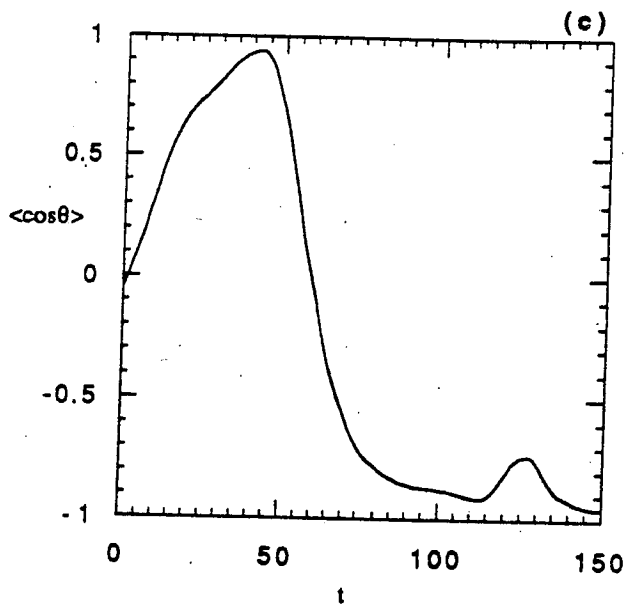
(c)
1
0.5
<cosθ>
0
-0.5
-1
0
50
100
150
t

Fig 14

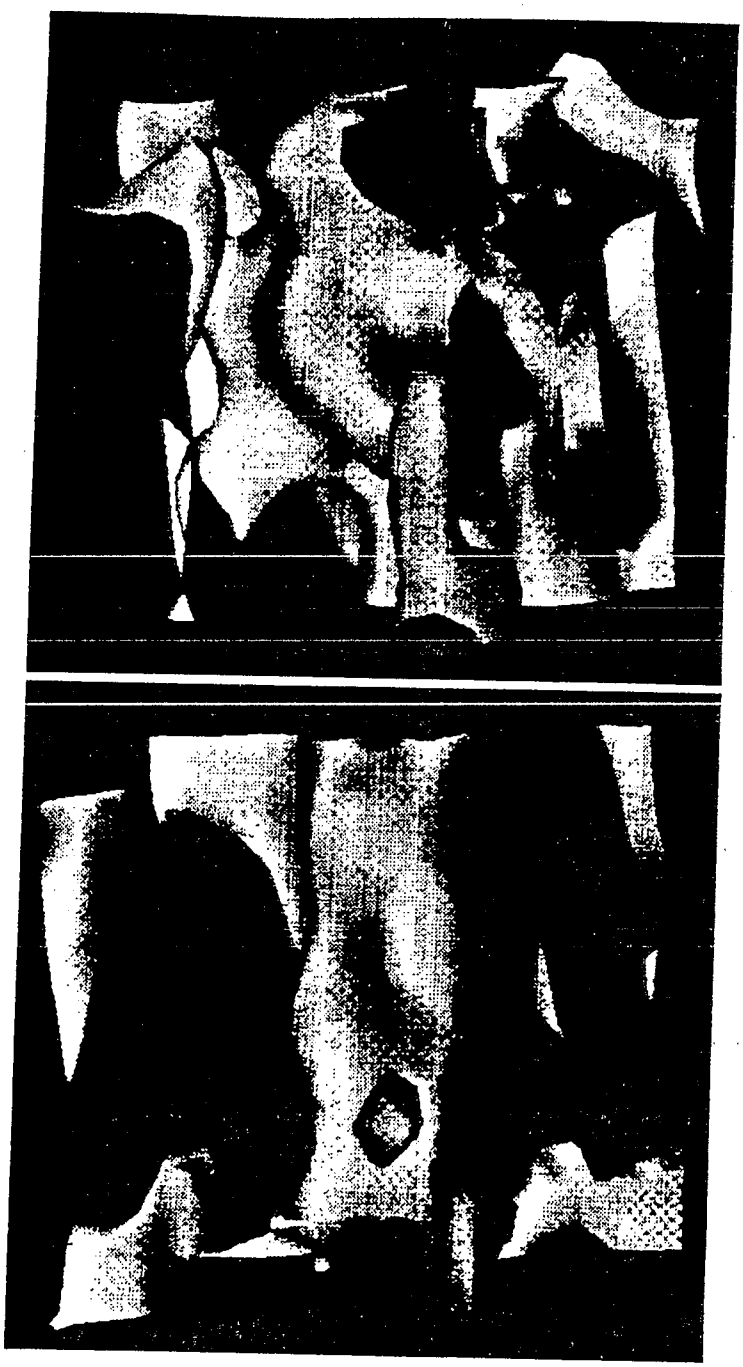

Fig 15

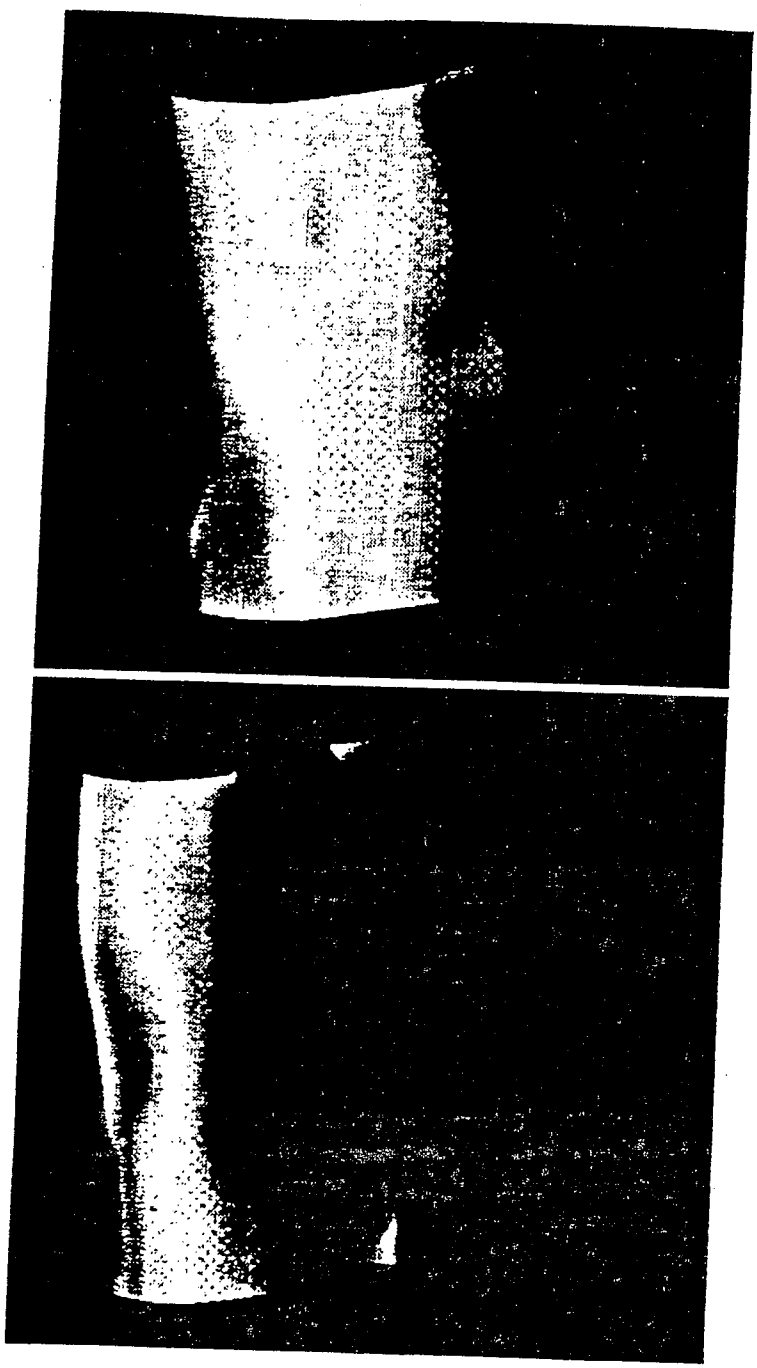

Fig 16